The Singlet−Triplet Absorption and Photodissociation of the HOCl, HOBr, and HOI Molecules Calculated by the MCSCF Quadratic Response Method

Boris F. Minaev

Department of Physics and Measurement Technology, Linköping University, S-58183, Linköping, Sweden

*Received: January 19, 1999; In Final Form: June 8, 1999*

The molecular absorption spectra of hypochlorous, hypobromous, and hypoiodous acids have been studied by multiconfiguration self-consistent field (MCSCF) calculations with linear and quadratic response techniques. The complete form of the spin−orbit coupling (SOC) operator is accounted. The singlet−triplet transition to the lowest triplet state $^3A'' \leftarrow X^1A'$ is shown to be responsible for the weak long-wavelength tail absorption and photodissociation in these molecules. The transition is polarized along the O−X bond (X = Cl, Br, I) and has an oscillator strength equal 6×10^{-6}, 8×10^{-5}, and 2×10^{-4} for hypoclorous, hypobromous, and hypoiodous acids, respectively. The second singlet−triplet transition $^3A' \leftarrow X^1A'$ comes to the region of the first singlet−singlet $^1A'' \leftarrow X^1A'$ absorption and contributes significantly to the total cross-section at wavelengths $\lambda \approx 300–320$ nm (X = Cl), $\lambda \approx 340–360$ nm (X = Br), and $\lambda \approx 400$ nm (X = I). In the last case the singlet−triplet transition $^3A' \leftarrow X^1A'$ produces predominant contribution to HOI absorption in the visible region. All states are dissociative, so the singlet−triplet absorption contributes to the yield of photolysis in the important near-UV and visible region close to the intense solar actinic flux. Contributions to the removal mechanisms for atmospheric HOCl, HOBr, and HOI species are shortly discussed. The minor loss process of ozone in troposphere because of the HOI reservoir sink is getting evident on the ground of this calculations. The importance of SOC accounting for atmospheric photochemistry problems is stressed.

I. Introduction

During the last 2 decades it has become increasingly evident that halogen-containing compounds have a great impact on stratospheric ozone. The monoxides of the halogens, XO (X = Cl, Br, I) are central to the chemistry that occurs.[1,2] Hypochlorous, hypobromous, and hypojodous acids, HOCl, HOBr, and HOI, play an important role in the atmospheric chemistry of the halogen oxide radicals and in the ozone depletion.[3−7,1,2] The role of these molecules in photochemistry of upper atmosphere is highly dependent on their photolysis in the long wavelength region ($\lambda \geq 300$ nm). For example, the photodissociation of HOCl

$$HOCl + h\nu \rightarrow HO(^2\Pi) + Cl(^2P) \quad (1)$$
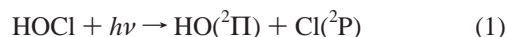
leads to an effective ozone depletion processes through the chain[1,6,7]

$$OH + O_3 \rightarrow HO_2 + O_2 \quad (2)$$

$$Cl + O_3 \rightarrow ClO + O_2 \quad (3)$$
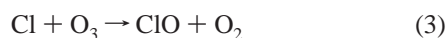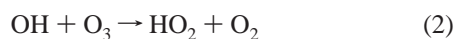
and a recombination of the products of the reactions 2 and 3 reproduces hypochlorous acid again

$$HO_2 + ClO \rightarrow HOCl + O_2 \quad (4)$$
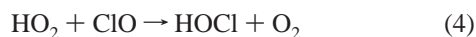
Thus the net reaction $2O_3 \rightarrow 3O_2$ occurs. The reaction 3 together with the process 5

$$ClO + O \rightarrow Cl + O_2 \quad (5)$$

provide a route for consumption of odd oxygen that can significantly add to the direct Chapman reaction

$$O + O_3 \rightarrow O_2 + O_2 \quad (6)$$

The chain length of the cyclic processes 3 and 5 is limited by termination reactions that remove the chain carriers Cl and ClO; the most important of these reactions are the formation of $ClONO_2$ (from ClO and NO_2) and the formation of HCl (from atomic chlorine and methane). These products are reservoirs for active chlorine rather than the final sinks, because other reactions can release catalytically active species again.[2]

Similar processes are connected with HOBr photolysis.[2−4] Recent measurements indicate that the ozone depletion potential for bromine is even greater than that of chlorine (on a per molecular basis).[4,8] Hypobromous acid is produced in the atmosphere both by gas-phase reaction

$$HO_2 + BrO \rightarrow HOBr + O_2 \quad (7)$$
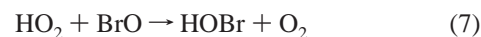
and by heterogeneous reactions involving the hydrolysis of $BrONO_2$ on aerosol particles in the night time stratosphere[8]

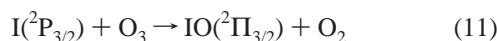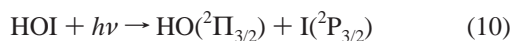$$H_2O + BrONO_2 \rightarrow HOBr + HNO_3 \quad (8)$$

A similar reaction between water vapor and $ClONO_2$ analogous species generate HOCl molecule in the stratosphere. Together with reaction,[4] this reaction complex constitutes an important source of atmospheric hypochlorous acid.[5,6] Important sequence of these reaction schemes is that hypobromous acid can couple ozone destructive cycles involving bromine with those involving chlorine and OH radicals.[4,9]

The number of investigations of the final member of this series, HOI, is far fewer; although, the hypoiodous acid too is treated as an important species in the chemistry of atmospheric iodine.[10−13] Significant levels of CH_3I in the troposphere are a

result of oceanic algal activity.[2] Atmospheric iodine is almost exclusively of biogenic origin. The CH$_3$I is rapidly photolysed by solar radiation, so that the potential exists for IO chemistry to play some part in tropospheric processes. The solar radiation that has not been absorbed in the Hartley band of ozone, that is a part of visible region (380−430 nm) which penetrates to the troposphere, can induce important photochemical processes with iodine containing compounds. The analogous reaction of reactions 4 and 7 for the iodine oxide radical was proposed as a source of HOI.[14]

$$HO_2 + IO(^2\Pi_{3/2}) \rightarrow HOI + O_2 \qquad (9)$$

The continual production and photolysis of gaseous hypoiodous acid by the reaction sequence eqs 9−11

$$HOI + h\nu \rightarrow HO(^2\Pi_{3/2}) + I(^2P_{3/2}) \qquad (10)$$

$$I(^2P_{3/2}) + O_3 \rightarrow IO(^2\Pi_{3/2}) + O_2 \qquad (11)$$

is believed to provide a minor loss process for ozone in the troposphere. The CH$_3$I may also be sufficiently long lived for some transport up to the stratosphere.[2,11] As with bromous analogous, the inorganic reservoirs of HOI and IONO$_2$ are rapidly photolyzed. The influence of iodine photochemistry on ozone concentrations in the lower stratosphere has been considered by Solomon et al.;[11] they stressed the important role of reaction 9 and the possible reactions of IO with other halogen monoxides.

Since reactions of the type (1) for all molecules HOCl, HOBr, and HOI are the rate-determining steps of the chain, an accurate determination of the UV absorption cross-section of hypochlorous, hypobromous, and hypoiodous acids is necessary for assessing the role of these molecules in the photochemical reaction cycles in the atmosphere.[4,6,7] That is why the UV absorption spectrum of HOCl has been the subject of many experimental[2,5−7,15−20] and theoretical[3,21−28] studies. Spectroscopic data on hypobromous acid are sparse, although recent studies by Orlando and Burkholder[29] and by Barnes et al.[4] have provided an accurate measurements of its absorption in the near-UV and visible region. The gas phase ultraviolet and visible absorption spectrum of HOI has been studied by Jenkin during the modulated photolysis of flowing H$_2$O$_2$ + I$_2$ mixtures.[2,14] The UV−vis absorption spectrum of HOI has also been studied in the aqueous phase.[30] The infrared spectrum of hypoiodous acid was recently investigated in gas phase in detail.[10,13]

The HOCl and HOBr molecules have intense absorption in the near-UV region. The maxima at $\lambda \simeq 240$ nm (HOCl) and $\lambda \simeq 280$ nm (HOBr) are much stronger than the longer wavelength peaks at $\lambda \simeq 300$ nm (HOCl) and $\lambda \simeq 350$ nm (HOBr).[2] In contrast to the spectra of hypochlorous and hypobromous acids, the absorption spectrum of HOI molecule has an intense first peak in the visible region at 410 nm and the weaker second peak at 335 nm.[2,14] Behind these very prominent qualitative differences, there are some very weak absorption features in the long wavelength tails of HOCl and HOBr molecules, which are of principal importance for the proper interpretation of the electronic spectra of the whole halogen-hydroxide series.

A big difficulty in recording the electronic absorption spectra of HOCl and HOBr molecules is determined by interference from strong absorption bands of Cl$_2$O and Br$_2$O radicals, respectively. These species are typically present in large concentrations as part of the source chemistry required to generate such unstable molecules as HOCl and HOBr; thus, the contribution of Cl$_2$O and Br$_2$O radicals to the hypochlorous and

hypobromous acids absorption spectra is difficult to eliminate.[4,20,67] For example, many experimental studies[6,7,16,18] have used the same basic method for generating gaseous HOCl; this is an equilibrium mixture of dichlorine monoxide and water vapor

$$H_2O + Cl_2O \rightarrow 2HOCl \qquad (12)$$

The problem is that the equilibrium constant of this reaction is very low (0.08−0.09 at 298 K).[15,18] As a result of the limited pressure of water vapor, the complete conversion of Cl$_2$O to HOCl cannot be achieved at normal temperature. The presence of Cl$_2$O contaminates the absorption spectrum since the dichlorine monoxide is a very strong absorber in the UV region where vapor of hypochlorous acid also absorbs. Molina et al.[6,7] and Knauth et al.[18] recorded the absorption spectrum of dichlorine monoxide and subsequently added water vapor to the optical cell. After equilibration was attained, the spectrum of the mixture was recorded and any changes relative to the pure spectrum of Cl$_2$O were attributed to HOCl formation. The equilibrium constant for reaction 12 and the absorption cross-section for HOCl were determined simultaneously by varying the concentration ratio for the reagent. Though the equilibrium constant has larger effect on the HOCl spectrum in the short wavelength region, it still influences the absorption measurements at $\lambda \geq 300$ nm, which is particular important for interpretation of the present theoretical study.

The reported spectra of HOCl molecule[5,7,15,18−20] are quite different in the whole region of wavelengths and in particular at the UV-A tail, $\lambda \geq 320$ nm. Molina et al.[6] obtained a very weak shoulder starting at $\lambda \simeq 400$ nm which strongly depends on the equilibrium constant of the reaction.[7] This shoulder almost disappears in the spectrum presented by Mishalanie et al.[15] The uncertainty depends on some additional products which could occur in the reaction.[5] Burkholder have combined the UV absorption spectra recorded following photolysis of the same equilibrium mixtures[12] with the infrared ν_2 band intensity measurement in the HOCl molecule; therefore, the HOCl concentration was calibrated by the IR spectrum.[20] The UV absorption spectrum from Burkholder's measurements displayed a maximum at 242 nm with a cross-section $\sigma = (2.1 \pm 0.3) \times 10^{-19}$ cm^2 and a secondary peak at 304 nm, $\sigma = 0.6 \times 10^{-19}$ cm^2. This spectrum was in excellent agreement with that of Knauth et al.[18] but was in poor agreement with other measurements.[6,15,19] The cross-sections of Permien et al.[19] have been adopted by the NASA as the recommended values for stratospheric modeling.[2] Some recent measurements presented in ref 2 are in agreement with the Burkholder's data.[20] It should be stressed that Burkholder assigned a larger absorption cross-section in the long-wave region 340−380 nm and presented some weak irregular absorption features in that part of the spectrum.[20]

Analysis of the long-wave tail absorption in all three molecules would be worth to start with the hypobromous acid spectrum. Orlando and Burkholder[29] were able to minimize the problem of HOBr absorption spectra contamination by careful background subtraction; they obtained an accurate absorption cross-section even for the overlapping spectral region 240−400 nm. Barnes et al.[4,5] have used an alternate method of recording an absorption-like spectrum of photodissociating molecules. They monitor the yield of a particular (OH) photofragment while scanning the wavelength of the incident light. A new absorption band (~400−500 nm) of hypobromous acid centered at 440 nm was detected by this method and tentatively assigned to a triplet state of HOBr.[4] Although the

peak absorption cross-section is very weak $\sigma_{max} \sim 10^{-21}$ cm^2, its influence on the photochemical lifetime of hypobromous acid is great due to proximity of the 440 nm region to the peak of the solar actinic flux.[4] The model of sudden ozone depletion in the Arctic troposphere[8] includes uncertainties in the HOBr photolysis rates; this hampers the assessment of the bromine chemistry contribution to Arctic ozone loss. An additional important contribution of the singlet−triplet long wavelength absorption to HOBr photolysis rate may have serious implications for the ozone depletion model.[4]

The singlet−triplet absorption of HOCl at the long wavelength tail ($\lambda \geq 350$ nm)[5,28] is of similar importance. Theoretical results for singlet−singlet transitions[21−23] and some early measurements,[1,6,15] indicate negligible HOCl absorption at wavelengths longer than 300 nm. The ozone molecule itself has a sufficiently strong absorption at $\lambda \leq 300$ nm.[1,32,33] If the conclusion of ref 21 is correct, the HOCl molecule would be stable to photodissociation if it is formed in the lower and middle stratosphere (below 50 km) where the solar UV radiation is attenuated by ozone at wavelengths shorter than 300 nm. In that case HOCl would be an inert reservoir for stratospheric chlorine.[21] A significant fraction of stratospheric chlorine might indeed be found in the form of HOCl if the reaction 4 is faster than the photolysis reaction 1 and other reactions of HOCl with OH, Cl, and O radicals.[6,15] The rate constant of reaction 4, $k_4 = (4−6) \times 10^{-12}$ cm^3/molecules, is higher than the rate constants of HOCl decomposition reactions with radicals.[2,15] The stratospheric photodissociation rate of reaction 1 estimated by Jaffe and DeMore[16] is sufficiently fast to make HOCl unimportant as an inert reservoir for stratospheric chlorine. This is in accord with the absorption cross-section measurements by Molina et al.[6,7] and by others[15,18,20] indicating that absorption beyond 300 nm is sufficiently strong.

Ab initio calculations[24−27] of the HOCl photoabsorption cross-section are in semiqualitative agreement with the experiment.[7,15] From calculations of Nanbu et al.[25] it follows that the singlet−singlet absorption spectrum of HOCl consists from an intense peak at about 250 nm (mostly the $2^1A' \leftarrow 1^1A'$ transition, with a calculated vertical excitation energy of 5.16 eV) and a shoulder with a maximum at about 300 nm (the $1^1A'' \leftarrow 1^1A'$ transition, with a calculated vertical excitation energy of 4 eV). All theoretical studies[3,21−25,28] predict that the first singlet−singlet $1^1A'' \leftarrow 1^1A'$ transition probability is significantly smaller than that for transition to the $2^1A'$ state. It is important to stress that *the calculated*[25−27] *singlet−singlet absorption intensity at 290−330 nm (the $1^1A'' \leftarrow 1^1A'$ transition) is significantly lower than the experimental measured cross-section*.[7,15,18−20] It was claimed recently[28] that the second singlet−triplet transition produces an important additional contribution to the UV absorption cross-section in this region. The most recent and accurate theoretical calculations of the singlet−singlet absorption cross-section in the UV-A region (320−400 nm)[25−27] are in agreement with measurements of Mishalaine et al.[15] but contradict the spectra recorded by Knauth et al.[18] and Burkholder.[20] It seems that the agreement is accidental; the results of ref 15 underestimate absorption in the UV-A region, and theoretical studies[25−27] consider only the singlet−singlet transitions. The authors of the ref 28 tried to assign the weak absorption in the range 360−380 nm recorded in some experimental studies[6,7,18,20] to the first singlet−triplet transition of hypochlorous acid. Since the paper[28] has been published, some new important results have been reported[5,34,35] for the HOCl molecule. In this paper we shall briefly recapitulate the results of the HOCl molecular study[28] with some new additional calculations and present

comparative analysis of HOBr and HOI spectra with particular attention to the role of the S−T transitions in photodissociation of hypochlorous, hypobromous, and hypoiodous acids. It will be shown that absorption by the first and second excited triplet states of hypohalous acids makes a nonnegligible contribution to the overall atmospheric photochemical activity of these molecules. By taking into account the importance of the $T−S_0$ transitions in ozone itself,[33,36−38] the involvement of the triplet states in the chemistry of the recombination and photodissociation processes $O_3 \rightleftharpoons O + O_2$,[39] one can make the general conclusion that photochemistry of the triplet states should be an important, additional, issue in the stratospheric ozone problem. The present results suggest that atmospheric photochemistry of the heavy halogen (bromine and, particularly, iodine) containing compounds would strongly depend on the radiative and nonradiative singlet−triplet transitions; therefore, relativistic effects should be taken in proper account.

II. Method of Calculations

The multiconfigurational self-consistent field (MCSCF) calculation in a complete active space (CAS) is a general background of the computational scheme[40−43] implemented in the present work. The correlated MCSCF reference wave function is used for the response theory treatment of the singlet−singlet (S−S) and singlet−triplet (S−T) transitions. The S−S transitions are calculated by linear response (LR) method.[40,41] The poles of the response function[40] give the excitation energies and the residues at the excitation frequency give the S−S transition moments to the corresponding excited states. The S−T transitions are forbidden in the nonrelativistic approximation, but spin−orbit coupling (SOC) mixes the spin multiplicity and gives rise to a nonvanishing transition dipole moment. There has been a number of ab initio studies of the S−T transition probabilities, see, for example, refs 43−46. A typical approach has been to describe the spin−orbit coupling perturbation in terms of a selected set of intermediate states and performing explicit summations over the intermediate states. The $S_0−T_1$ transition dipole moment connected with a particular spin sublevel k is determined in this case by the well-known equation

$$M_l(T^k) = \langle \tilde{S}_0|r^l|\tilde{T}_1^k\rangle =$$
$$\sum_n \frac{\langle S_0^0|r^l|S_n^0\rangle\langle S_n^0|H_{so}^k|T_1^{k,0}\rangle}{E(T_1^0) - E(S_s^0)} + \sum_m \frac{\langle S_0^0|H_{so}^k|T_m^{k,0}\rangle\langle T_m^{k,0}|r^l|T_1^{k,0}\rangle}{E(S_0^0) - E(T_m^0)} \quad (13)$$

where H_{so}^k is the kth component ($k, l \in x, y, z$) of the SOC operator (T_1^0 and $\tilde{T}_1$ denote the zero and first order wave functions of perturbation theory). It is useful to employ Cartesian triplet components (zero field splitting, ZFS-spin functions) which are related to the spherical components (high external magnetic field, HEMF-spin functions) by the irreducible tensor transformation[43]

$$T^x = \frac{T^{-1} - T^1}{\sqrt{2}} \quad T^y = i\frac{T^{-1} + T^1}{\sqrt{2}}, T^z = T^0 \quad (14)$$

Each spin sublevel of the triplet state T^k is associated with a specific S−T transition probability.

It was noted[44,47,46] that convergence of the S−T transition moment row, eq 13, in configuration interaction (CI) treatment is very slow. Many terms in the sum-over-state expansion, eq 13, are of similar magnitude but of different signs.[43,47] Vahtras et al.[42] have proposed to use the response theory and demon-

strated[48] that the matrix element of eq 13 is associated with the residue of a quadratic response (QR) function at the excitation frequency of the S−T transition. The sum-over-state expression, eq 13, in MCSCF QR theory of the S−T transition moment is replaced by solutions of sets of linear equations.[42] Since these solutions can be determined using direct iterative techniques of the response equations, large dimensions and therefore large orbital and configuration space MCSCF wave functions can be considered. Therefore, errors from truncation of the slowly converged expansions, employed in conventional procedures, is completely avoided. The method used is fully analytical and can be seen as an analytic analogue of a finite field calculation of the dipole transition moment from an MCSCF linear response calculation where the spin−orbit operator represents the applied field. The MCSCF QR method employs the operators associated with describe the effect of an external perturbation.[43] By allowing the orbitals to relax in the response to the external field, the requirements to the CI expansion is reduced. Both orbital excitation operators and configuration excitation operators describe correlation. Conventional configuration interaction approaches use only the latter, and call for more elaborate calculations to obtain an equal correlation level. The restricted CI method also leads to size-consistency errors when the S−T transition dipole moment is studied as a function of vibrational displacements or as a function of reaction coordinate. Different molecular geometries can lead to different sets of configuration state functions and also to different patterns of summation in the truncated row (eq 13).

Calculations of spectral properties of HOCl, HOBr, and HOI molecules have been performed by MCSCF QR method with account of few basis sets and complete active spaces (CAS) patterns. The correlation-consistent basis sets of Dunning et al.[49] have been widely used for HOCl molecule. The polarized valence double-ζ (cc-pVDZ) basis set was formerly imploied in photodissociation and S−T transitions intensity calculations of HOCl molecule.[28] Basis sets of Sadlej[50] and Ahlrichs et al. (VDZ and VTZ)[51] and Dunning's triple-ζ (cc-pVTZ) basis set, as well as the augmented (aug-cc-pVDZ) basis set, are also used for comparison for geometry optimization and for spectral properties study. It was found here that the aug-cc-pVDZ basis set is adequate for the both singlet−triplet transitions study in the HOCl molecule. For HOBr molecule the basis set of Sadlej[50] and VDZ set of Ahlrichs et al.[5] as well as the 3-21G basis set of Pople et al.[52] were employed. The HOI molecule was calculated with the 3-21G basis set[52] only. For comparison of the vertical excitations in both molecules we shall concentrate attention on the results obtained in the Sadlej's and Ahlrich's VDZ basis sets. Though the VDZ basis set of Ahlrichs et al.[51] is quite moderate (for light atoms) and overestimates bond lengths at MCSCF level of geometry optimization, it gives the S−T transition moments in quantitative agreement with the results obtained with the cc-pVDZ and cc-pVTZ basis sets of Dunning et al.[49] for HOCl molecule.[28] The most intense $T_1 \leftarrow S_0$ transitions are obtained for the T^z spin sublevel; for all basis sets studied in previous work[28] these transition dipole moments are very close to values 0.008 and 0.002 au for y and z polarization, respectively.[28] Finally, comparative analysis of all hypohalous acids (HOCl, HOBr, and HOI) spectra is made on the 3-21G level of theory, which is shown to be relevant for semiqualitative purposes. The S−T transitions intensity is well reproduced on the 3-21G level in comparison with much more flexible basises.

A full form of the spin−orbit coupling operator,[43] including one- and two-electron terms, was employed. The choice of axes
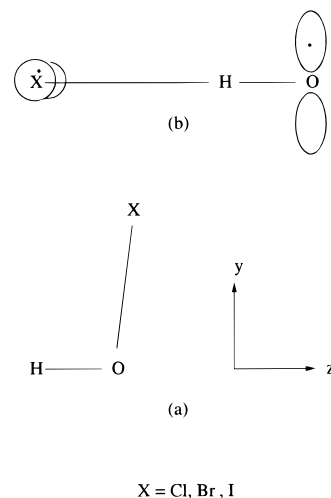
X = Cl, Br, I

Figure 1. (a) Choice of axes for the HOCl, HOBr, and HOI molecules; (b) the biradical structure of the equilibrium lowest triplet state.

for all HOX molecules (X = Cl, Br, I) is given in Figure 1a. At the equilibrium ground state geometry the Hartree−Fock electronic configuration (Sadlej basis set) of HOCl molecule is

$$1^1A'(HOCl) = (core)^{12}(6a')^2(7a')^2(8a')^2(2a'')^2(9a')^2(10a')^2(3a'')^2 \quad (15)$$

The corresponding ground state configuration of HOBr and HOI molecules look like the following

$$1^1A'(HOBr) = (core)^{30}(12a')^2(13a')^2(14a')^2(5a'')^2(15a')^2(16a')^2(6a'')^2 \quad (16)$$

and

$$1^1A'(HOI) = (core)^{48}(18a')^2(19a')^2(20a')^2(8a'')^2(21a')^2(22a')^2(9a'')^2 \quad (17)$$

In all MCSCF calculations the core orbitals were set inactive. For few trial sets of MCSCF calculations all other occupied MOs (five orbitals of a′ symmetry and two orbitals of a″ symmetry) and three empty MOs (2,1) have been included in the complete active space (14 electrons in 10 orbitals) which corresponds to 7232 determinants of $^1A'$ symmetry for the reference ground state. Here and in the following the notation (n, m) refers to the number of orbitals of (a′, a″) symmetry in the complete active space. Exclusion of the lowest occupied valence orbital (6a′ MO in HOCl, 12a′ MO in HOBr, and 18a′ MO in HOI molecule) with low energy (~-1.39 au) does practically not influence the results of spectral calculations. So almost all calculations were performed in a CAS with six MOs of the a′ type and three MOs of the a″ type (12 electrons in nine MOs). This CAS (6,3) includes 3560 determinants for the reference ground state. The extension of the empty MOs is very unreasonable from two points of view: the three lowest empty orbitals, included in this CAS, are pretty well separated in energy from a large group of quasi-degenerate MOs which occur in all basis sets. The same trend is seen from the natural orbital occupation numbers obtained by MP2 calculations. Furthermore, attempts to increase CAS by extension of a number of empty orbitals lead to physically unreasonable S−T transition moments of about 1 au (may be because of a poor balance from different quasi-degenerate state contributions). Transition energies to the nine lowest excited states calculated by MCSCF linear response

method are quite close in all the tested CAS spaces and are similar to results of other recent calculations.[3,25]

We have used the same approximation for estimation of the absorption cross-section $\sigma(\nu)$ which was introduced in ref 21. Only the O−X bond length dependence (X = Cl, Br, I) of the transition moments is taken into account.

$$\sigma(\nu) = \frac{8\pi^3\nu^3}{3hc}\sum_{v=0}^{n}F_v\sum_{l,k}|\int_{1.6}^{2.6}\Psi_{E_f}(r_{O-X})M_l^k(r_{O-X})\Psi_v(r_{O-X})dr_{O-X}|^2 \tag{18}$$

Here ν is the frequency of the transition (cm^{-1}), E_f is an energy of the final (upper) dissociative state, Ψ_{E_f} is the upper state continuum wave function, M_l^k is the electronic transition dipole moment between the initial (ground singlet state) and the final triplet T^k state determined by eq 13, Ψ_v is a vibrational wave function of the ground state, F_v is the fraction of ground state molecules in the vth vibrational level. The limits of integration are in angstroms.

At frequency ν the upper state turning point r_0 is defined as the value of r_{O-X} (X = Cl, Br, I) which satisfies $\nu = E_f(r_0) - E_v$, where $E_f(r_0)$ is the energy of the final state relative to the ground state equilibrium geometry.[21] The MCSCF-calculated energy gradients are used for numerical estimations of the integral 18 with an account of the Airy function approach.[21] The leading term in this expansion is simply the "reflection" approximation for bound-continuum transitions.[21] The Boltzmann-averaged cross-section at 300 K is given in the following discussion.

Formally determined oscillator strength (f) for the T ← S absorption calculated with the electronic transition moment of eq 13

$$f_l = \frac{8\pi^2 mc\nu}{3he^2}\sum_k|M_l(T^k)|^2 \tag{19}$$

without an account of nuclear wave functions is also presented in the tables. Assuming that the Franck−Condon factor is equal to unit for the vertical T ← S transition from the bound to the dissociative state, this formally determined oscillator strength is a rough measure of the absorption intensity at the maximum of the T−S band.

In addition to previous study of HOCl molecule[28] the extended geometry variations for excited states dissociation reaction paths by grid points have been done here. The MCSCF QR and LR calculations with the experimental ground state geometry also have been performed and then the potential energy curves, the singlet−singlet and singlet−triplet transition moments as functions of the O−X distance at the fixed experimental ground state geometric parameters for the ∠HOX angle and for the O−X bond length were studied. These calculations have been done with the (aug-cc-pVDZ) basis set of Dunning et al.[49] for HOCl molecule (Figures 2−4) and with the Sadlej basis set for the HOBr molecule (Figures 5−7). The 3-21 basis set results are presented in Figures 8−10 for the HOI molecule.

III. Results and Discussion

A. Energetics of the Ground and Excited States. Dissociation Paths. Geometry optimization of HOCl molecules have been performed by the MCSCF method with CAS (6,3) in six different basis sets; three basis sets have been used for HOBr
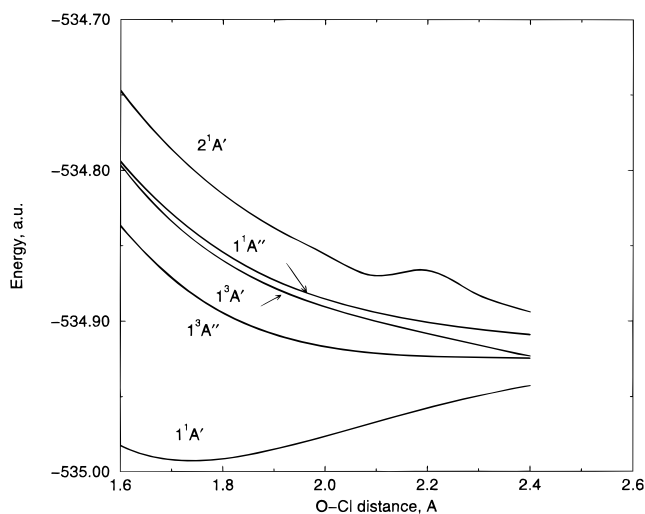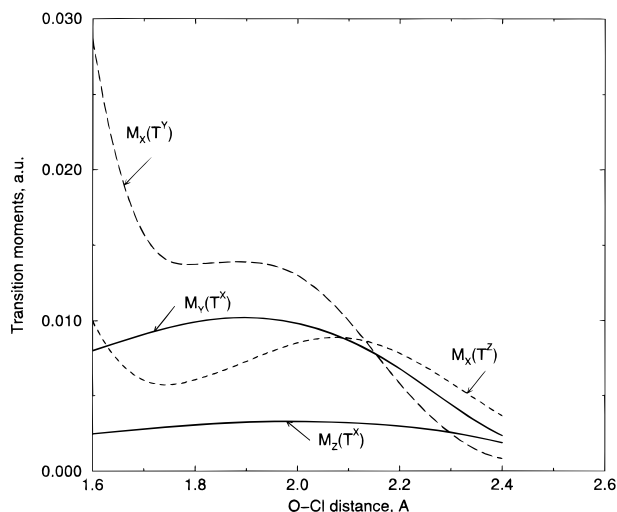

Figure 2. O−Cl bond length dependence of the total energies for the ground and few excited states in the HOCl molecule calculated by the MCSCF LR method in the aug-cc-pVDZ basis set.
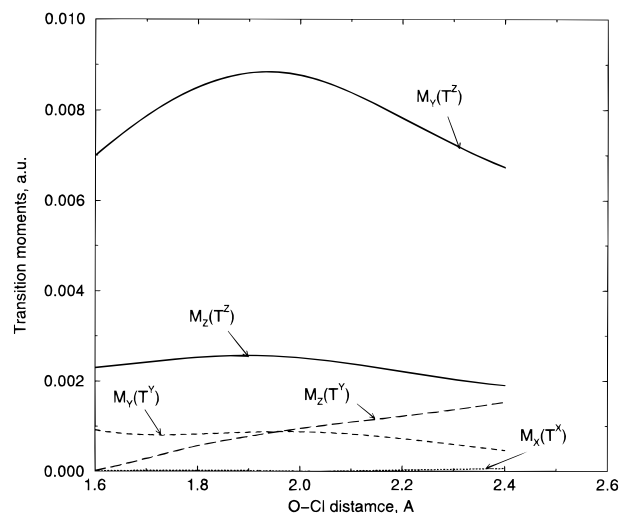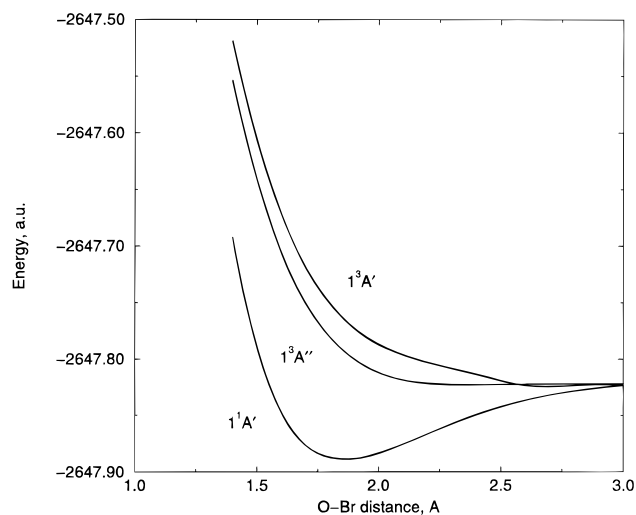

Figure 3. O−Cl bond length dependence of the T_1 ← S_0 transition dipole moment in the HOCl molecule calculated by the MCSCF QR method in the aug-cc-pVDZ basis set.

molecule optimization in the same CAS. The results of the MCSCF geometry optimization in the ground and in the first excited triplet state of the HOCl, HOBr, and HOI molecules are presented in Tables 1 and 2, respectively, together with experimental and other theoretical data. For the ground state all methods predict similar results which are quite close to the experimental bond lengths and infrared (IR) frequencies. The IR intensities of the ground state HOCl molecule obtained in this work in the basis set of Sadlej[50] are in a good agreement with the results of recent coupled cluster CCSD(T) calculations of Lee.[53] A similar geometry of HOCl molecule has been optimized by Nanbu and Iwata,[25] but they obtained a rather strange bending vibration frequency (344 cm^{-1}). The basis sets of Ahlrichs et al.[51] slightly overestimate bond lengths and underestimate the IR intensity of the O−H stretching vibration in the HOCl molecule. Only very recent accurate CCSD(T) calculations in a very big basis[34,35] give the O−Cl distance close to the experimental value 1.69 Å[54] and also reproduce the ∠HOCl angle. The dissociation energy (D_e) of hypochlorous acid in respect to Cl(^{2}P$_{3/2}$) + OH($^2\Pi_{3/2}$) cleavage obtained with the aug-cc-pVDZ basis set is equal to 51.3 kcal/mol; this should be compared with the recent very accurate prediction D_e = 62.3

Figure 4. O—Cl bond length dependence of the $T_2 \leftarrow S_0$ transition dipole moment in the HOCl molecule calculated by the MCSCF QR method in the aug-cc-pVDZ basis set.

Figure 6. O—Br bond length dependence of the $T_1 \leftarrow S_0$ transition dipole moment in the HOBr molecule calculated by the MCSCF QR method in the basis set of Sadlej.

Figure 5. O—Br bond length dependence of the total energies for the ground and the two lowest triplet states in the HOBr molecule calculated by the MCSCF LR method in the basis set of Sadlej.
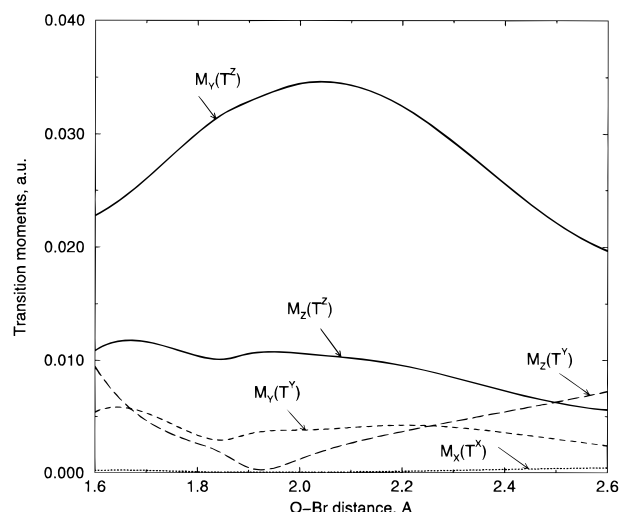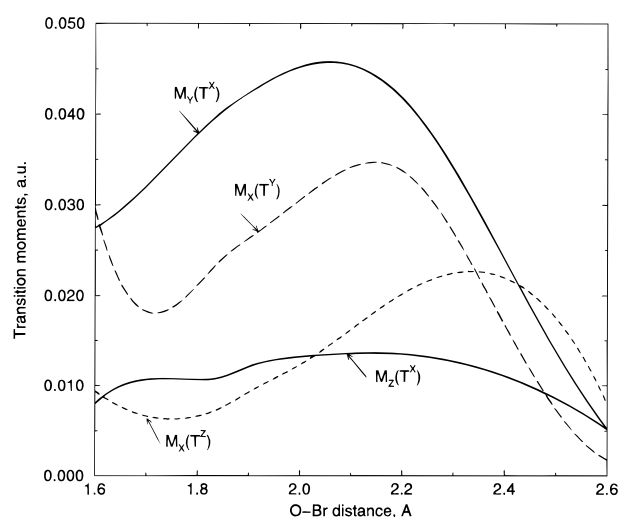

Figure 7. O—Br bond length dependence of the $T_2 \leftarrow S_0$ transition dipole moment in the HOBr molecule calculated by the MCSCF QR method in the basis set of Sadlej.

kcal/mol.[35] It is interesting to note that the MNDO CI method[55] gives the heat of formation of HOCl molecule (-16.98 kcal/mol) in excellent agreement with experimental data[6,7] and also reproduces the ground state geometry ($r_{OH} = 0.95$ Å, $r_{OCl} = 1.683$ Å, $\angle HOCl = 106.7°$) quite reasonale (see Table 1). MNDO CI results were used in this work for a preliminary study and qualitative interpretation of the spectra.

The O—H bond in the hypobromous acid is slightly shorter than in the hypoclorous acid; all methods reproduce this delicate trend (Table 1). The O—Br bond is longer than the O—Cl bond by 0.15 Å; this difference is not so large in our calculations (0.06–0.1 Å). The O—I bond is longer than O—Br bond by 0.157 Å, and the 3-21G basis reproduces this difference pretty well (0.163 Å). The lowest excited triplet state $1^3A''$ and $1^3A'$ of all three molecules are repulsive in the Franck–Condon region in the vicinity of the vertical excitation from the ground $1^1A'$ state. At the ground state internuclear distances the $^3A''$ state is bent, while the $^3A'$ state is linear. The bending potential is very soft in both triplet states. This angle dependence obtained by the linear response (LR) method[43] for HOCl molecule[28] is reproduced also for HOBr species in basis set of Sadlej. The dissociative behavior of the five lowest singlet excited states and of the two triplet states obtained in this work by MCSCF

LR calculations for HOBr molecule is very similar to that obtained before for HOCl molecule.[21,28] The five studied low-lying excited states of HOCl, HOBr, and HOI molecules are all bound with respect to the O—H stretch. Our search by grid points in LR MCSCF method (VDZ basis set of Ahlrichs et al.[51]) indicates that the low-lying triplet states $^3A''$ and $^3A'$ must dissociate to OH + X products (X = Cl, Br). Though the both triplet states can dissociate, in principle, to the O(^3P) + HX products (this asymptote is lower in energy than vertical excitations, but slightly higher than the OH + X limit for both molecules), the starting acceleration of fragments will prevent the O + HX formation in a primary photochemical step. The lowest $1^3A''$ triplet starts to dissociate in a bent structure, while the second excited triplet state, $1^3A'$, undergoes fast linearization along the dissociation path. Similar behavior is obtained for HOI molecule in 3-21G basis set calculations. At this point we do not pay attention to different spin—orbit components ratio for the dissociation products OH($^2\Pi_J$):X(^2P_J); this work is under the progress.

MCSCF (aug-cc-pVDZ) potential energy curves for the $1^1A'$ and $1^3A''$ states along the dissociation reaction coordinate (elongation of the O—Cl bond at the fixed O—H distance r_{O-H}
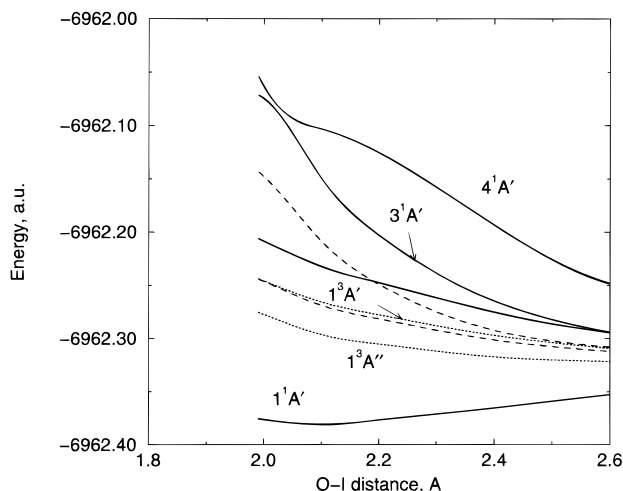
Figure 8. O−I bond length dependence of the total energies for the ground and few lowest excited singlet and triplet states in the HOI molecule calculated by the MCSCF QR method in the 3-21G basis set. The $^1A'$ states are denoted by solid lines, the $^1A''$ states are denoted by dashed lines, and the triplet states are denoted by dotted lines.

Figure 9. O−I bond length dependence of the $T_1 \leftarrow S_0$ transition dipole moment in the HOI molecule calculated by the MCSCF QR method in the 3-21G basis set.

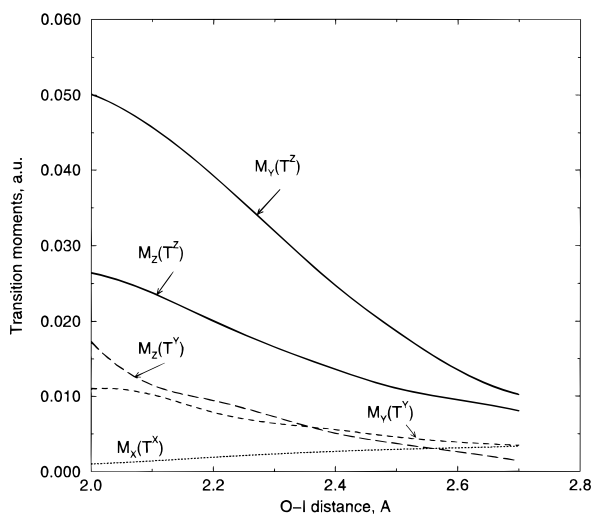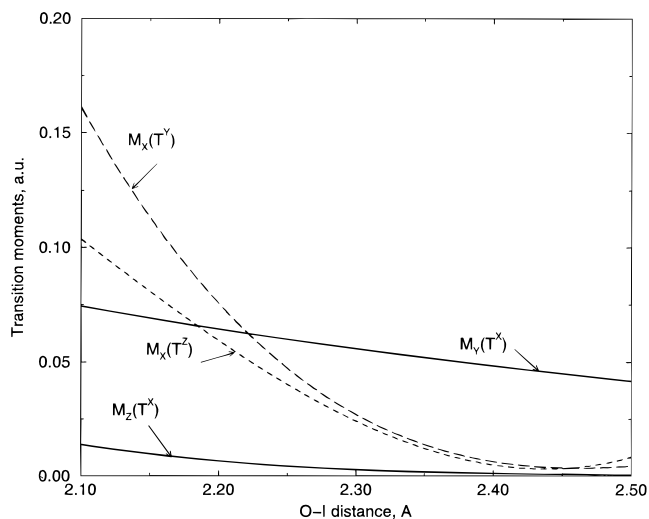**Figure 10.** O−I bond length dependence of the $T_2 \leftarrow S_0$ transition dipole moment in the HOI molecule calculated by the MCSCF QR method in the 3-21G basis set.

= 0.98 Å and angle ∠HOCl = 100.8°) are shown in Figure 2. There is a very weak minimum on the lowest triplet state curve at r_{O-Cl} = 3.75 Å with a dissociation energy D_e = 0.06 kJ/mol. The minimum is well seen on a large scale curve. This is not a real minimum on the triplet state potential energy hypersurface (PEHS) since the angle and the O−H bond were fixed (∠HOCl = 100.8°); but still it indicates a tendency to arrange a weak associate between Cl and OH moieties as a triplet state radical pair. From Figure 2 one can see that the lowest triplet curve is very flat at large O−Cl distances so the system is getting flexible at $r_{O-Cl} \geq$ 2.1 Å. Complete geometry optimization at the same MCSCF level gives the angle ∠ClHO = 180°, so the Cl atom migrates to the other side of the OH radical when the O−Cl bond is getting weak (Table 2). Only the 3-21G basis predicts a nonlinear triplet bound state with stretched O−Cl bond (2.47 Å), Table 2. A similar result has been obtained on the Hartree−Fock level earlier.[56] The MCSCF geometry optimizations of the $1^3A''$ state with flexible basis sets predict the linear structure with the chlorine atom wriggled out of the oxygen bonding. This is a tightly bound radical pair Cl• + HO• with D_e = 2.6 kJ/mol. The Cl−H distance in this triplet state molecule (radical pair) is about 3 Å. The electronic

structure of this system is represented in Figure 1b. The relative stability of the linear ClHO molecule in the triplet state could be easily understood in terms of the arguments presented by Goddard et al.[57] considering 3 π_x and 3 π_y electrons, as in the O_2 molecule. Just the same result has been obtained by MCSCF geometry optimization of the lowest triplet $1^3A''$ state in the HOBr system with larger basis sets than 3-21G (Table 2). The last basis does not predict a bound triplet state. For this reason the search for the triplet state geometry optimization in the HOI molecule has not been performed, since the 3-21G basis cannot reproduce weak intermolecular interaction in such systems (Table 2). But we can anticipate that the bound radical pair I• + HO• should also exist; a strong SOC contribution will produce an additional stabilization of this heavy system. The predicted XHO triplet structure near the dissociation limit hardly has any importance for the photodissociation process since the X and OH fragments pass through this region with high velocity. But this triplet state of the radical-pair-like structure (Figure 1b) could definitely be important for the recombination reaction $X(^2P)$ + OH and for the process described by eq 4.

Triplet state collisions of two radicals occur more often because of the statistical weights ratio (3:1) in comparison with the singlet state. The weakly bound triplet radical pair (Figure 1b) being formed at slow collision conditions in the cold stratosphere is a metastable spin trap. It has few quasi-degenerate states with very large spin−orbit coupling (SOC) matrix elements between the singlet and triplet counterparts. The reactive singlet ground state $1^1A'$ (Figure 3) is 0.022 eV below the stable $1^3A''$ triplet radical pair. The SOC between these two states is zero; the second triplet $1^3A'$ state is 0.081 eV above the singlet and has a big SOC matrix element with both singlet and triplet states. For the Br−HO complex the SOC matrix element $\langle 1^1A'|H_{SO}^x|1^3A'\rangle$ = 964 cm^{-1} as calculated by LR MCSCF method in VDZ basis. Both triplets are mixed by bending vibrations and by SOC. It means that the T $\rightsquigarrow$ S intersystem crossing can occur leading to the total enhancement of the recombination rate and yield.

The disproportionation reactions (reactions 4, 7, and 9) must proceed on the triplet state PEHS since the products HOX + O_2 are in the total triplet state (HOX has the singlet ground state and O_2 has the triplet ground state). The separated radical pair HO_2 + XO could be either in the singlet or in the triplet state. The intermediate triplet state consisting from two triplet

HOCl, HOBr, and HOI Molecules

J. Phys. Chem. A, Vol. 103, No. 36, 1999 **7301**

TABLE 1: MCSCF Geometry Optimization for the Ground Singlet States $1^1A'$ of the HOCl, HOBr, and HOI Molecules. r Is the Internuclear Distance (angstroms), ν Is the Vibrational Harmonic Frequency (cm^{-1}). IR Intensities (km/mol) in Parentheses; E_n Is the Total Energy (hartree) of the nth State

method	r_{O-H} (Å)	r_{O-X} (Å)	$\angle HOX^i$	ν_1,O–H	ν_2,bend	ν_3,X–O	E_n (hartree)
				HOCl			
3-21G[a]	1.0098	1.8705	99.62	3318.4(7.05)	1247.6(50.8)	596.2(3.8)	−532.353270
AhlrichsVDZ[a]	1.0029	1.8941	100.41	3406(37.9)	1182.0(43.91)	567.7(1.8)	−534.714626
AhlrichsVTZ[a]	0.9941	1.8690	102.2	3467.8(21.9)	1206.6(41.8)	578(0.66)	−534.970471
cc-pVDZ[a]	0.9785	1.75175	100.65	3708(62.1)	1274.4(36.5)	668(0.02)	−534.97653
aug-cc-pVDZ[a]	0.9761	1.7446	101.37	3719.7(59.9)	1288.9(38.9)	698.0(2.63)	−534.992847
Sadlej[a]	0.9784	1.7450	101.2	3718.9(60.5)	1284.5(38.5)	693(2.83)	−535.005587
MRCI[b]	0.9640	1.6960	102.66	3804.3	1275.4	734.0	−535.44035
CCSD(T)[c]	0.964	1.723	101.7	3802(63)	1274.0(41)	704(4)	−535.33348
CCSD(T)[d]	0.9641	1.6918	102.85	3618.8	1243.5	729.6	−535.46159
exptl[e]	0.9644	1.6890	102.96	3794	1272	739.3	
				HOBr			
3-21G[a]	1.0076	1.9410	101.92	3334.6(8.3)	1226.1(41.4)	534.5(3.5)	−2635.115489
AhlrichsVDZ[a]	1.0002	1.9530	103.59	3434.4(52.85)	1185.5(33.4)	506.3(2.18)	−2647.473917
Sadlej[a]	0.967	1.849	102.82	3918.0(59.1)	1181.5(31.5)	603(2.3)	−2647.889613
CISD[f]	0.955	1.842	102.8	3991	1233	653	−2648.01040
MRCISD[f]	0.966	1.897	100.1				−2647.91641
CCSD(T)[f]	0.964	1.884	100.9	3837	1180	573	−2648.06638
CCSD(T)[g]	0.964	1.853	102.3	3807	1197	608	−2648.22065
exptl[h]	0.961	1.834	102.3	3792	1194.2	629.7	
				HOI			
3-21G[a]	1.0078	2.1044	103.73	3329.6(11.95)	1176.3(35.6)	484.6(3.6)	−6962.380763
exptl[h]	0.964	1.991	105.4	3625.8	1068	575	

^{a} This work. MCSCF in (6a′,3a″) CAS. ^{b} Reference 35. Multireference CI in the aug-cc-pVQZ basis set of Dunning et al.[49] augmented with some diffuse AOs. ^{c} Reference 53. Coupled-cluster method with singles, doubles, and partly triple excitations in the TZ2P basis. ^{d} Reference 34. Coupled-cluster method with singles, doubles, and partly triple excitations in the cc-pV5Z basis set of Dunning et al.[49] ^{e} Reference 35. ^{f} Reference 3. ^{g} Reference 66. ^{h} Reference 65.

TABLE 2: MCSCF Geometry Optimization for the Lowest Triplet States $1^3A''$ of the HOCl and HOBr Molecule. r Is the Internuclear Distance (Å), ν Is the Vibrational Harmonic Frequency (cm^{-1}). IR Intensities (km/mol) Given in Parentheses; E_n Is the Total Energy (hartree) of the nth State

method	r_{O-H} (Å)	r_{O-X} (Å)	$\angle HOX^j$	ν_1, O–H	ν_2,bend	ν_3,X–O	E_n (hartree)
				HOCl			
3-21G[a]	1.0180	2.4678	93.39	3195.75(15.34)	497.93(150.38)	171.47(23.2)	−532.2930882
AhlrichsVDZ[a]	1.0067	3.8552[c]	0	3369(4.2)	161.8(161.3)	73.8(0.3)	−534.666087
AhlrichsVTZ[a]	0.9991	4.0954[c]	0				−534.921446
cc-pVDZ[a]	0.9829	3.9834[c]	0	3655.7(19.2)	121.4(123.6)	52.9(0.12)	−534.907913
HF, 6-31G(d)[b],	0.959	3.009	104.9				−534.83284
				HOBr			
3-21G[a]	1.0173	8.9802[d]	0	3171.27(32.62)			−2635.03885
AhlrichsVDZ[a]	0.9763	3.9880[c]	0	3761.8(42.09)	145.86(195.00)	59.39(0.15)	−2647.37918
Sadlej[a]	0.9852	4.0059[c]	0	3358.2	138.2	52.3	−2647.80453

^{a} This work. MCSCF in (6a′,3a″) CAS. ^{b} Reference 56. ^{c} This structure corresponds to the linear XHO complex with $r_{X–H} \sim 3$ Å. ^{d} With the 3-21G basis set geometry optimization of the lowest triplet state leads to dissociation to OH + Br.

molecules XHO and O_2 can play the role of a spin trap which finally passes through the T ⤳ S transition inside the XHO moiety in order to produce separated products of the reactions (reactions 4, 7, and 9).

Linear response calculations for the two triplet states $^3A''$ and $^3A'$ along the dissociation reaction coordinate (elongation of the O–X bond at the fixed O–H distance $r_{O–H} = 0.98$ Å and angles $\angle HOCl = 101°$ and $\angle HOBr = 102°$ and $\angle HOI = 103.7°$) give physically reasonable solutions for all distances except for very long O–X separations (for example, $r_{O–Cl} \geq 3$ Å). In this region the LR method gives some nonregular behavior. This region will not be treated here since it does not contribute to the photoabsorption cross-section. The MCSCF ground state potential energy curves (PEC) in all three molecules are smooth along the whole reaction coordinate as well as the singlet excited states PEC obtained by the LR method. We shall use the quadratic response (QR) method for calculations of the $1^3A'' \leftarrow 1^1A'$ and $1^3A' \leftarrow 1^1A'$ transitions dipole moments in the vicinity of the Franck–Condon region.

Results are presented in Tables 3–4 and in Tables 5–6, respectively. Summary for the whole spectra calculations is given in Table 7.

B. Selection Rules for the T_1-S_0 ($1^3A'' \to 1^1A'$) Transitions. In HOX molecules the triplet–singlet transitions to three spin sublevels of the triplet state have different intensities and polarizations, which follows simple selection rules.[28] The triplet state spin sublevels, eqs 9–11, transform as irreducible representations of rotations around the symmetry axes; in the C_S point group they do it in the following way:

$$T^x \in A' \tag{20}$$

$$T^y, T^z \in A'' \tag{21}$$

The electric dipole moment ($\mathbf{M} = e\sum_i \mathbf{r}_i$) transforms as a translation along the axes:

$$M_x \in A'' \tag{22}$$

$$M_y, M_z \in A' \tag{23}$$

So we have the following selection rule: I. Transition $1^3A'' \leftarrow 1^1A'$ to the x spin sublevel is x polarized (x axis is perpendicular to the molecular plane). The x spin sublevel of the triplet state

TABLE 3: $T_1 \leftarrow S_0$ Transition in the HOCl Molecule. MCSCF Quadratic Response Calculations of the Vertical Triplet−Singlet Transition Moment $M_a(T^b) = \langle 1^1A' | e\sum_i a_i | 1^3A''(T^b) \rangle$ (in 10^{-6} au) at the Averaged Equilibrium Geometry in the Ground State $r_{O-Cl} = 1.75$ Å, $r_{OH} = 0.98$ Å, $\angle HOCl = 100.8°$. $\Delta E_{S,T}$ Is the Transition Energy, f_a Is the Oscillator Strength for the $T_1 \leftarrow S_0$ Absorption Polarized along the a Axis

$M_a(T^b)$	3-21G	cc-pVDZ	cc-pVDZ^a	aug-cc-pVDZ^b	Ahlrichs	Sadlej
$M_x(T^x)$	110	73	81	18	167	4
$M_y(T^y)$	564	581	586	815	336	580
$M_z(T^y)$	179	8183	292	545335		335
$M_y(T^z)$	6621	7713	7709	7788	8276	8591
$M_z(T^z)$	2424	2222	2217	2404	2493	2268

Transition Energy (eV) and Oscillator Strength

$\Delta E_{S,T}$ (eV)	3.23	3.01	3.01	3.36	3.22	2.91
f_x	9.6×10^{-10}	3.7×10^{-10}	4.5×10^{-10}	2.7×10^{-11}	8×10^{-10}	3×10^{-13}
f_y	3.5×10^{-6}	4.4×10^{-6}	4.5×10^{-6}	5.05×10^{-6}	5.4×10^{-6}	5.3×10^{-6}
f_z	4.4×10^{-7}	4.9×10^{-7}	4.9×10^{-7}	4.8×10^{-7}	5.1×10^{-7}	3.7×10^{-7}
f_{total}	3.94×10^{-6}	4.8×10^{-6}	4.9×10^{-6}	5.5×10^{-6}	5.9×10^{-6}	5.7×10^{-6}

^{a} Extended CAS (7a′,3a″; 14 electrons in 10 MOs). ^{b} Calculated at the experimental ground state geometry.

TABLE 4: $T_1 \leftarrow S_0$ Transition in the HOBr Molecule. MCSCF Quadratic Response Calculations of the Vertical Transition Moment $M_a(T^b) = \langle 1^1A' | e\sum_i a_i | 1^3A''(T^b) \rangle$ (in 10^{-6} au) at the Averaged Equilibrium Geometry in the Ground State $r_{O-Br} = 1.85$ Å, $r_{OH} = 0.96$ Å, $\angle HOBr = 102.3°$. $\Delta E_{S,T}$ Is the Transition Energy, f_a Is the Oscillator Strength for the $T_1 \leftarrow S_0$ Absorption Polarized along the a Axis

$M_a(T^b)$	3-21G	AhlrichsVDZ	AhlrichsVDZ^a	Sadlej
$M_x(T^x)$	715	620	707	53
$M_y(T^y)$	2605	2122	1843	2904
$M_z(T^y)$	4137	6499	6866	1690
$M_y(T^z)$	23477	3077	31542	31813
$M_z(T^z)$	9888	11756	11888	10099

Transition Energy (eV) and Oscillator Strength

$\Delta E_{S,T}$ (eV)	3.07	2.92	2.90	2.64
f_x	3.84×10^{-8}	2.74×10^{-8}	3.55×10^{-8}	1.82×10^{-10}
f_y	4.19×10^{-5}	6.8×10^{-5}	7.06×10^{-5}	6.6×10^{-5}
f_z	6.63×10^{-6}	1.29×10^{-5}	1.34×10^{-5}	6.78×10^{-6}
f_{total}	4.86×10^{-5}	8.09×10^{-5}	8.4×10^{-5}	7.28×10^{-5}

^{a} Extended CAS (7a′,3a″; 14 electrons in 10 MOs).

TABLE 5: $T_1 \leftarrow S_0$ Transition in the HOI Molecule. MCSCF Quadratic Response Calculations with the 3-21G Basis Set of the Vertical Transition Moment $M_a(T^b) = \langle 1^1A' | e\sum_i a_i | 1^3A''(T^b) \rangle$ (in 10^{-6} au) at the Experimental (exptl) and at the o (opt) Equilibrium Geometry in the Ground State. $\Delta E_{S,T}$ Is the Transition Energy, f_a Is the Oscillator Strength for the $T_1 \leftarrow S_0$ Absorption Polarized along the a Axis

$M_a(T^b)$	(exptl)^a	(opt)^b	(opt)^{b,c}
$M_x(T^x)$	1005	1466	1121
$M_y(T^y)$	11174	10127	10242
$M_z(T^y)$	17733	11359	11495
$M_y(T^z)$	50407	45466	45168
$M_z(T^z)$	26695	23631	23527

Transition Energy (eV) and Oscillator Strength

$\Delta E_{S,T}$ (eV)	2.73	2.28	2.29
f_x	6.74×10^{-8}	1.20×10^{-7}	7.05×10^{-8}
f_y	1.78×10^{-4}	1.21×10^{-4}	1.20×10^{-4}
f_z	6.85×10^{-5}	3.85×10^{-5}	3.84×10^{-5}
f_{total}	2.46×10^{-4}	1.60×10^{-4}	1.59×10^{-4}

^{a} Experimental equilibrium geometry in the ground state: $r_{O-I} = 1.991$ Å, $r_{OH} = 0.9643$ Å, $\angle HOI = 105.4°$. ^{b} Optimized equilibrium geometry in the ground state: $r_{O-I} = 2.104$ Å, $r_{OH} = 1.0078$ Å, $\angle HOI = 103.73°$. ^{c} Extended CAS (7a′,3a″; 14 electrons in 10 MOs).

has a zero spin projection on the x axis, so both nonpaired spins are precessing in the molecular plane. II. Transitions $1^3A'' \leftarrow 1^1A'$ to the y and z spin sublevels each have their particular in-plane polarization. Our choice of y, z axes is not arbitrary; it is very close to the directions of the magnetic axes determined by the zero-field splitting (ZFS) Hamiltonian, which accounts for intramolecular magnetic interactions: spin−spin coupling and SOC (in the second order).[47] The orientation of the y and z ZFS axes is slightly changed along the dissociation reaction coordinate, but it is still close to that choice shown in Figure 1a. This is important for analysis of the spin alignment in the dissociation products.

C. T_1-S_0 ($1^3A'' \leftarrow 1^1A$) Transitions in the HOCl, HOBr, and HOI Molecules. The MCSCF QR results of the $1^3A'' \leftarrow 1^1A'$ vertical transition moment calculations in the HOCl, HOBr, and HOI molecules are presented in Tables 3, 4, and 5, respectively. The transition is determined mostly by the 11a′ ← 3a″ single-electron excitation in HOCl, by the 17a′ ← 6a″ excitation in HOBr, and by the 23a′ ← 9a″ excitation in HOI. This is $\sigma^*_{O-X} \leftarrow \pi^*_{O-X}$ transition. Its singlet counterpart (the $1^1A'' \leftarrow 1^1A'$ transition) has a low intensity since the σ^*_{O-X} MO bears small s-character on oxygen and especially on the X atom.[47] The T_1-S_0 transition intensity depends mostly on the p character of the σ^*_{O-X} MO on the X atom[47] since this quantity determines spin−orbit coupling with a number of low lying singlet states. The transition moments dependence on the O−Cl distance calculated in aug-cc-pVDZ basis set of Dunning et al.[49] is given in Figure 3 for the HOCl molecule. These results are quite similar to transition moments, presented before,[28] which were obtained from the cc-pVDZ basis set at slightly different geometry of OH fragment. (Equilibrium ground state O−H bond length and angle $\angle HOCl$ 102.96° were fixed along the dissociation reaction.) The potential energy curves along this reaction coordinate for HO + Cl dissociation are presented in Figure 2. These PECs are very similar to the curves previously obtained with the cc-pVDZ basis set and given in Figure 3 of ref 28; the important difference is connected with the splitting between the T_2 and S_1 states energy.

All transition moments for the $T_1 \leftarrow S_0$ absorption in the HOBr molecule calculated from the basis set of Sadlej are given in Figure 6; the vertical transition characteristics are presented in Table 4 for few basis sets and active spaces used. The HOI results (3-21G) are given in Figure 9 and Table 5.

We shall start with transitions determined by the selection rule II, since they are much more intense in all three molecules.

1. T_1-S_0 ($1^3A'' \leftarrow 1^1A'$) Transitions to the y and z Spin Sublevels. From the above selection rules it follows that there are four transition moments in this band: two for each spin sublevel. It follows from Figures 3, 6, and 9 that for the studied

HOCl, HOBr, and HOI Molecules

J. Phys. Chem. A, Vol. 103, No. 36, 1999 **7303**

TABLE 6: $T_2 \leftarrow S_0$ Transition in the HOCl Molecule. MCSCF Quadratic Response Calculations of the Vertical Triplet−Singlet Transition Moment $M_a(T^b) = \langle 1^1A'|e\sum_i a_i|1^3A'(T^b)\rangle$ (in 10^{-6} au) at the Averaged Equilibrium Geometry in the Ground State $r_{O-Cl} = 1.75$ Å, $r_{OH} = 0.98$ Å, ∠HOCl = 100.8°. $\Delta E_{S,T}$ Is the Transition Energy, f_a Is the Oscillator Strength for the $T_2 \leftarrow S_0$ Absorption Polarized along the a Axis

$M_a(T^b)$	3-21G	cc-pVDZ	cc-pVDZ^a	aug-cc-pVDZ^b	Ahlrichs	Sadlej
$M_y(T^x)$	7853	9370	9485	8994	9309	10053
$M_z(T^x)$	2096	2586	2630	2757	2171	2708
$M_x(T^y)$	2765	2824	3891	15252	9389	15907
$M_x(T^z)$	1890	1151	1604	5797	4876	5516

			Transition Energy (eV) and Oscillator Strength			
$\Delta E_{S,T}$ (eV)	4.59	4.10	4.11	4.39	4.33	3.90

	3-21G	cc-pVDZ	cc-pVDZ^a	aug-cc-pVDZ^b	Ahlrichs	Sadlej
f_x	7.53×10^{-7}	9.34×10^{-7}	1.78×10^{-6}	2.86×10^{-5}	1.19×10^{-6}	2.71×10^{-5}
f_y	6.95×10^{-6}	8.81×10^{-6}	9.06×10^{-6}	8.69×10^{-6}	9.20×10^{-6}	9.66×10^{-6}
f_z	4.95×10^{-7}	6.72×10^{-7}	6.97×10^{-7}	8.17×10^{-7}	5.00×10^{-7}	7.01×10^{-7}
f_{total}	8.2×10^{-6}	1.04×10^{-5}	1.15×10^{-5}	3.82×10^{-5}	2.16×10^{-5}	3.74×10^{-5}

^{a} Extended CAS (7a′,3a″; 14 electrons in 10 MOs). ^{b} Calculated at the experimental ground state geometry.

TABLE 7: $T_2 \leftarrow S_0$ Transition in the HOBr Molecule. MCSCF Quadratic Response Calculations of the Vertical Transition Moment $M_a(T^b) = \langle 1^1A'|e\sum_i a_i|1^3A'(T^b)\rangle$ (in 10^{-6} au) at the Averaged Equilibrium Geometry in the Ground State $r_{O-Br} = 1.85$ Å, $r_{OH} = 0.96$ Å, ∠HOBr = 102.3°. $\Delta E_{S,T}$ Is the Transition Energy, f_a Is the Oscillator Strength for the $T_2 \leftarrow S_0$ Absorption Polarized along the a Axis

$M_a(T^b)$	3-21G	AhlrichsVDZ	AhlrichsVDZ^a	Sadlej
$M_y(T^x)$	34317	40892	40677	40395
$M_z(T^x)$	8001	8666	8646	10977
$M_x(T^y)$	43932		72558	24173
$M_x(T^z)$	23349		32871	7638

		Transition Energy (eV) and Oscillator Strength		
$\Delta E_{S,T}$ (eV)	4.16	3.81	3.73	3.43

	3-21G	AhlrichsVDZ	AhlrichsVDZ^a	Sadlej
f_x	2.52×10^{-4}		5.8×10^{-4}	5.4×10^{-5}
f_y	1.20×10^{-4}	1.56×10^{-4}	1.51×10^{-4}	1.37×10^{-4}
f_z	6.53×10^{-6}	7.02×10^{-6}	6.84×10^{-6}	1.01×10^{-5}
f_{total}	3.78×10^{-4}		7.38×10^{-4}	2.01×10^{-4}

^{a} Extended CAS (7a′,3a″; 14 electrons in 10 MOs).

range of the O−X bond distances (1.6−2.7 Å) the transitions to the z spin sublevel are the most intense (see also Tables 3−5). For these transitions to the z spin sublevel, the absorption probabilty is determined by integrals:

$$M_a(T^\varepsilon) = \langle 1^1A'|e\sum_i a_i|1^3A''(T^\varepsilon)\rangle \qquad (24)$$

where $a \in y, z$ are in-plane axes. The singlet−triplet excitations to both y and z spin sublevels can borrow intensity from spin-allowed $n^1A'-1^1A'$ transitions because of the SOC mixing

$$\langle n^1A'|H_{so}^b|1^3A''(T^b)\rangle \qquad (25)$$

In eq 25 $b \in y, z$. The most intense singlet−singlet (S−S) absorption in the near UV region ($\lambda \sim 240$ nm) is determined by the $2^1A'-1^1A'$ transition which has polarization close to the O−Cl axis in the HOCl molecule; similar results are obtained for the HOBr and HOI molecules. Not only this transition but also higher S−S excitations produce large contributons of the same sign to the integral of eq 24.

Important contributions come also from the triplet−triplet (T−T) transitions $1^3A''-m^3A''$ by SOC induced interaction between the ground singlet and the mth excited triplet m^3A'' states

$$\langle 1^1A'|H_{so}^b|m^3A''(T^b)\rangle \qquad (26)$$

where $b \in y, z$. The largest contribution to the integral eq 24

and to the total $T_1 \leftarrow S_0$ absorption in all three molecules is connected with $a = y$ (polarization almost along the O−X bond) and is determined by the intensity borrowing from the $n^1A'-1^1A'$ transitions (see $n = 4$ in Table 7) in the far UV region.

In the case $n = m = 1$, there is a particular contribution from the difference of the permanent dipole moments $\Delta\mu$ of the S_0 and T_1 states.[28] The SOC integral eq 26, $m = 1$, is equal to 160.9 cm^{-1} ($b = z$) and 37.8 cm^{-1} ($b = y$) for the equilibrium geometry of the HOCl molecule; the corresponding SOC values for the HOBr molecule are 891.5 cm^{-1} ($b = z$) and 217 cm^{-1} ($b = y$). The appreciable admixture of the triplet $1^3A''(T^z)$ character into the singlet $1^1A'$ ground state and vice versa could lead, in principle, to a large contribution to the transition moment.[13,24] But the difference $\mu(S_0)-\mu(T_1)$ is small ($\mu(S_0)$ = 1.65 D in the ground state; $\mu(T_1)$ = 1.74 D in the triplet state for the HOCl molecule. $\mu(S_0)$ = 1.96 D and $\mu(T_1)$ = 2.09 D, respectively, for the HOBr molecule. So these $\Delta\mu$ contributions are small. Otherwise the transition moment should increase with the O−Cl distance, since the energy gap between these states goes to zero and the SOC integrals eq 26, $m = 1$, are still quite large (until $r_{O-X} \leq 2.7$ Å). The reason for that the transition moments $\langle 1^1A'|e\sum_i r_i|1^3A''(T^z)\rangle$ along y and z directions (solid lines in Figures 3, 6, and 9) are descending functions of the O−X distance is connected with the fact that the main contribution to these integrals originate in the SOC mixing between the triplet state $^3A''(T^z)$ and the highly excited singlet state $4^1A'$. The vertical S_0-S_4 excitation energy is about 9 eV with large transition moment $M_y = (0.7-1)$ au. The M_y integral increases until the distance $r_{O-X} \sim 2$ Å is reached and then decreases rapidly; this trend explains the behavior of the $S_0-T_1^\varepsilon$ transition moment with the in-plain directions. One can see that the $M_y(T^z)$ component is about 3 times larger than the $M_z(T^z)$ component at the maximum point (solid lines in Figures 3, 6, and 9), which means that the $M(T^z)$ transition dipole moment is oriented almost along the O−X axis. Only transitions to the T^z spin sublevel are the most intense in the vicinity of the Franck−Condon region; up to the bond length $r_{O-X} = 2.6$ Å, $M(T^z) \gg M(T^y)$ (Figures 5, 6, and 7). The vertical excitation corresponds almost to the peak on the transition moment curve in HOCl (Table 3, Figure 3) and also in HOBr (Table 4, Figure 6) and HOI (Table 5, Figure 9) molecules. This result determines a comparative importance of the $T_1 \leftarrow S_0$ absorption in the near-UV and visible region for the HOI, HOBr, and HOCl photolysis. From Figures 3, 6, and 9 one can see that the most important $M_y(T^z)$ transition moment is large even at long O−X distances: at $r = 2.6$ Å its value is 0.004 au in HOCl[28] and is about 0.02 au in HOBr and HOI species (Figures 6 and 9).

By taking into account overlap of the ground state vibrational wave function and the T_1 state nuclear continuum we can predict a long tail of the $T_1 \leftarrow S_0$ absorption, this tail should be especially long for the HOBr molecule since the value $|M_y(T^z)|^2$ is pretty big at large O–Br separation where the S–T transition energy is small and nuclear wave functions still have nonzero overlap. These findings are in good qualitative agreement with the experimental data of Barnes et al.[4,5] A very long weak tail of the $T_1 \leftarrow S_0$ absorption of HOBr spreads in the visible region until 650 nm.[4] Our results support the tentative assignment[4] and make it clear that the recent models of bromine chemistry in the Arctic troposphere[8] need more accurate definition of the HOBr absorption in visible region.

2. T_1–S_0 ($1^3A'' \leftarrow 1^1A'$) Transitions to the x Spin Sublevel. Intensity of this absorption with the out-of-plane polarization is practically negligible in all three molecules. The reason for this is the following. The out-of-plane polarized intensity is determined by the transition moment:

$$M_x(T^x) = \langle 1^1A'|e\sum_i x_i|1^3A''(T^x)\rangle \qquad (27)$$

It can borrow intensity from the singlet–singlet n^1A''–$1^1A'$ transitions because of the SOC mixing

$$\langle n^1A''|H^x_{so}|1^3A''(T^x)\rangle \qquad (28)$$

and from the triplet–triplet transitions $1^3A''$–m^3A' by SOC induced interaction between the ground singlet and the mth excited triplet m^3A' state.

$$\langle 1^1A'|H^x_{so}|m^3A'(T^x)\rangle \qquad (29)$$

The latter SOC integral for the second excited triplet T_2 state ($1^3A'$) with the vertical excitation energy 4.1 eV for the HOCl molecule and 3.7 eV for the HOBr molecule is quite large (132 cm^{-1} in HOCl and 1063 cm^{-1} in HOBr). It is almost constant in a wide range of geometry changes, being slightly increased at longer O–X distances. But perpendicular transitions of the A''–A' type (at low energies ≤ 9 eV) are not intense in both molecules neither in the S–S nor in the T–T manifolds. One of the most intense T–T transitions, the T_1–T_2 ($1^3A''$–$1^3A'$), has a comparatively large transition dipole moment. It is equal to 0.028 au in the HOCl molecule; its contribution to the integral eq 27 is 2.5×10^{-4} au (the second sum of eq 13 with $m = 2$). But even this contribution is quenched by other terms in the row (eq 13) so the final result is almost negligible $M_x(T^x) = 73 \times 10^{-6}$ au (Table 3, cc-pVDZ results for HOCl). This transition dipole moment corresponds to a negligible oscillator strength $f_x = 3.7 \times 10^{-10}$. Similar quenching occurs in the HOBr and HOI molecules. All values in the first row of Tables 3 and 4 are consistent with each other since they determine the absorption intensity which is, at least, 3 orders of magnitude lower than the absorption to other spin sublevels.

Although the transition dipole moment eq 27 increases along the dissociation path in the HOCl molecule (dotted line in Figure 3) and also in the HOBr and HOI species (Figures 6 and 9), its contribution to the cross-section of the $T_1 \leftarrow S_0$ absorption band is less than 10^{-23} cm^2 in the HOCl and HOBr molecules. It is slightly larger in HOI (6×10^{-23} cm^2), but still remains negligible. So there is no measurable absorption in the first $T_1 \leftarrow S_0$ band with perpendicular polarization. The $T_1 \leftarrow S_0$ transitions to other spin sublevels (mostly T^z), which have the in-plane polarization, are much more intense (Tables 3–5), and overwhelm the perpendicular component.

3. Angle Dependence of the $T_1 \leftarrow S_0$ ($1^3A'' \leftarrow 1^1A'$) Transition Moment and the Absorption Cross-Section. Comparison with Experiment. The $1^3A'' \leftarrow 1^1A'$ transition moment is almost parallel to the O–X bond (X = Cl, Br, I), and it follows this direction when the bond angle ∠HOX increases. There is only a rotation of the transition moment in the y,z plane. The length of the vector is only slightly diminished ($M^2 = 6.69 \times 10^{-5}$ (au^2) at ∠HOCl = 100.8°, $M^2 = 6.5 \times 10^{-5}$ (au^2) at ∠HOCl = 120°, and $M^2 = 6.17 \times 10^{-5}$ (au^2) at ∠HOCl = 130°). We can easily neglect these changes in the Franck–Condon region. Similar results are obtained for the HOBr and HOI molecules. The calculated absorption cross-section $\sigma(\nu)$ has a maximum $\sigma = 3.6 \times 10^{-21}$ cm^2 at $\nu \sim 23\,800$ cm^{-1} for the HOCl species and $\sigma = 4.4 \times 10^{-20}$ cm^2 at $\nu \simeq 22\,100$ cm^{-1} for the HOBr molecule (results correspond to the aug-cc-pVDZ basis for HOCl and to the basis set of Sadlej for HOBr). These are in semiquantitative agreement with recent measurements: $\sigma = 4 \times 10^{-21}$ cm^2 at $\nu \simeq 26\,300$ cm^{-1} for HOCl molecule[5] and $\sigma_{max} \sim 9 \times 10^{-21}$ cm^2 at $\nu \simeq 22\,700$ cm^{-1} for the HOBr molecule.[4] In HOI $\sigma = 7.6 \times 10^{-20}$ cm^2 at $\nu \simeq 21\,400$ cm^{-1}. The approach used for the estimation of the absorption cross-section[21] is very rough, and we skip the detailed presentation of these data. A more sophisticated method of wave packet propagation[27] is now under the progress. Some qualitative features could be mentioned in brief. Since the most intense $M_y(T^z)$ transition moment has a comparatively large value even at $r_{O-Cl} = 2.5$ Å, the overlap of the continuum nuclear wave functions in the upper state with the exponentially decaying tails of the ground state vibrational wave functions produces an appreciable contribution to the cross-section ($\sigma \sim 10^{-22}$ cm^2) even at $\nu = 22\,000$ cm^{-1} for the HOCl molecule. For the HOBr molecule the weak tail stretchs far in the visible region; at $\nu = 16\,000$ cm^{-1} the calculated cross-section is about 10^{-22} cm^2.

The HOCl molecule used in the experiments was not rotationally cooled[5,20,58,59] while the theory[21] has neglected the rotational quantum number. The model of photodissociation of a nonrotating molecule that treats the upper state dynamics with $J' = 0$ is not strictly physically correct since the $J = 0 \rightarrow J' = 0$ transition is forbidden.[27] The nonrotating model is equivalent to the assumption that the photodissociation dynamics are insensitive to the direction of polarization of the incident light.[27] Although the dynamic model of photodissociation used here is rather primitive and does not consider neither rotational nor electronic orbital- and spin-momenta, the MCSCF QR calculations are of better quality and permit to make a qualitative comparison with precise experiments.[5,58,59] The $T_1 \leftarrow S_0$ absorption band borrows intensity mostly from the UV transition $4^1A' \leftarrow 1^1A'$ which is very strong (Table 7) and has a polarization along the O–Cl bond direction (this is mostly the $\sigma^*_{O-Cl} \leftarrow \sigma_{O-Cl}$ excitation). Therefore the $T_1 \leftarrow S_0$ transition has the same polarization. It is connected mostly with the T^z spin sublevel (zero spin projection on the O–H direction) of the triplet state. These results are in perfect agreement with recent measurements of OH photofragment yields and of their Doppler line shapes.[5] Not only intensity of the $T_1 \leftarrow S_0$ absorption (the measured cross-section $\sigma = 4 \times 10^{-21}$ cm^2 [5]) but also polarization of the absorbing light obtained from the sub-Doppler spectroscopy (the O–Cl bond direction)[5] coincide with our results.

The S_2–S_0 ($2^1A' \leftarrow 1^1A'$) absorption in the HOCl molecule at 266 nm produces a spin alignment in favor of the $^2\Pi_{3/2}$ state of the OH fragment.[59] This is the $\sigma^*_{O-Cl} \leftarrow n_{Cl}$ excitation. It really correlates with the lowest component of the OH doublet $^2\Pi_{3/2}$ when SOC is taken into account along the dissociation

HOCl, HOBr, and HOI Molecules

J. Phys. Chem. A, Vol. 103, No. 36, 1999 **7305**

TABLE 8: $T_2 \leftarrow S_0$ Transition in the HOI Molecule. MCSCF Quadratic Response Calculations with the 3-21G Basis Set of the Vertical Transition Moment $M_a(T^b) = \langle 1^1A'|e\sum_i a_i|1^3A'(T^b)\rangle$ (in 10^{-6} au) at the Experimental (exptl) and at the Optimized (opt) Equilibrium Geometry in the Ground State. $\Delta E_{S,T}$ Is the Transition Energy, f_a Is the Oscillator Strength for the $T_2 \leftarrow S_0$ Absorption Polarized along the a Axis

$M_a(T^b)$	(exptl)^a	(opt)^b	(opt)^{b,c}
$M_y(T^x)$	75639	73877	75374
$M_z(T^x)$	13875	13456	13713
$M_x(T^y)$		156405	138677
$M_x(T^z)$		101633	91381

Transition Energy (eV) and Oscillator Strength			
$\Delta E_{S,T}$ (eV)	3.58	3.12	3.13
f_x		2.66×10^{-3}	2.12×10^{-3}
f_y	5.02×10^{-4}	4.17×10^{-4}	4.36×10^{-4}
f_z	1.69×10^{-5}	1.38×10^{-5}	1.44×10^{-5}
f_{total}		3.09×10^{-3}	2.57×10^{-3}

^{a} Experimental equilibrium geometry in the ground state: $r_{O-I} = 1.991$ Å, $r_{OH} = 0.9643$ Å, $\angle HOI = 105.4°$. ^{b} Optimized equilibrium geometry in the ground state: $r_{O-I} = 2.104$ Å, $r_{OH} = 1.0078$ Å, $\angle HOI = 103.73°$. ^{c} Extended CAS (7a′,3a″; 14 electrons in 10 MOs).

reaction path. Other features of the spin−orbit population ratios[58] are in qualitative agreement with our SOC calculations.

D. T_2-S_0 ($1^3A' \leftarrow 1^1A'$) Transitions in the HOCl, HOBr, and HOI Molecules. The second T−S transition in all molecules is almost 1 eV higher in energy than the first one (Table 9). So it comes to the region of the first S−S absorption and seems to be overwhelmed by the $1^1A'' \leftarrow 1^1A'$ band. In general the S−S transitions are usually much more intense than the S−T transitions. But this is not true for the $T_2 \leftarrow S_0$ ($1^3A' \leftarrow 1^1A'$) and $S_1 \leftarrow S_0$ ($1^1A'' \leftarrow 1^1A'$) transitions in the HOCl, HOBr, and HOI molecules. This is not an artifact of perturbation theory and QR approach. Although the energies of the T_2 ($1^3A'$) and S_1 ($1^1A''$) states are very close in the Franck−Condon region (Figures 2 and 8, see also Figure 3 of ref 28), the perturbation theory is still applicable for almost the whole region of the dissociation reaction coordinate, excluding very short O−X bond lengths. The lowest S_1-T_2 energy gap for the vertical excitations (400 cm^{-1}) has been obtained in the HOCl molecule with the cc-pVDZ basis set; it was getting very small (137 cm^{-1}) at r(O−Cl) = 1.97 Å.[28] This was comparable with the SOC matrix elements

$$\langle 1^1A''|H_{so}^b|1^3A'(T^b)\rangle \qquad (30)$$

which are equal 84.8 cm^{-1} for z spin sublevel and 159.3 cm^{-1} for y spin sublevel, so the perturbation theory cannot be applied. The S_1-T_2 energy gap is much higher in the aug-cc-pVDZ basis set (and also in the HOBr and HOI molecules), so the problem of applicability of perturbation theory does not occur for the equilibrium and longer O−X distances. Besides that, this SOC mixing is only important for the M_x components of the $T_2^{y,z}-S_0$ transitions, which are less intense than other vertical $T_2^x-S_0$ transitions in the HOCl molecule (Table 6, 3-21G and cc-pVDZ bases) and in the HOBr species (Table 6, basis set of Sadlej, Figure 11). Other results for the $M_x(T^{y,z})$ components should be considered with caution.

1. T_2-S_0 ($1^3A' \leftarrow 1^1A'$) Transitions to the y and z Spin Sublevels. According to eqs 21−24, these transitions have the out-of-plane (x) polarization and borrow intensity (partly) from the $n^1A'' \leftarrow 1^1A'$ transitions. In the cc-pVDZ basis set calculation[28] at the O−Cl distance near 1.97 Å, the T_2 ($1^3A'$) and S_1 ($1^1A''$) states are very close in energy. (See Figure 3 of

ref 28. The energy gap in cc-pVDZ basis is only 0.017 eV and perturbation treatment is doubtful at this point.) There is no S−T crossing between the T_2 ($1^3A'$) and S_1 ($1^1A''$) states in the cc-pVDZ basis set calculations for HOCl presented in Figure 3 of ref 28, as was mentioned before. The vicinity of this point (1.97 ± 0.16 Å) was excluded from the total intensity summation in cc-pVDZ basis set calculations,[28] since perturbation theory could not be applied. At this point the calculated transition dipole moment

$$M_x(T^b) = \langle 1^1A'|e\sum_i x_i|1^3A'(T^b)\rangle \qquad (31)$$

(where $b \in y, z$ are in-plane axes of spin quantization) was equal to 0.037 au for $b = y$ and to 0.026 au for $b = z$ in the HOCl molecule. These are the sharp maxima on the $M_x(T^{y,z})$ curves; the vicinity of the point (1.97 ± 0.16 Å) is excluded from the intensity summation procedure and substituted by the integral $1/\sqrt{2}\langle 1^1A'|e\sum_i x_i|1^1A''\rangle$, by taking into account that both transitions $S_1 \leftarrow S_0$ and $T_2 \leftarrow S_0$ share the same intensity at the region of quasi-degeneracy where SOC mixes both states. This sharing does not produce the total absorption intensity change in the region of quasi-degeneracy of the two states. But in other points of the dissociation coordinate the $S_1 \leftarrow S_0$ and $T_2 \leftarrow S_0$ transition energies do not coincide; the $T_2 \leftarrow S_0$ absorption has its own contribution to the absorption cross-section. For vertical $T_2 \leftarrow S_0$ transition (Table 6, cc-pVDZ basis) the considered integrals (eq 31) are much lower than the transition moments to other spin sublevel (T^x). The last values are determined by intensity borrowing from A′−A′ transitions and perturbation theory is perfectly applicable in these cases. These transitions are considered in the next section.

The perpendicular (x) polarized $T_2^{y,z} \leftarrow S_0$ transitions are not the most intense in all the region of geometry changes, except the region of vicinity of the tight approach of the T_2 ($1^3A'$) and S_1 ($1^1A''$) potential energy. In the cc-pVDZ basis set this region occurs at 1.97 Å; in larger basis sets (aug-cc-pVDZ and Sadlej basis sets, where the T_2 ($1^3A'$) and S_1 ($1^1A''$) states quaside-generacy does not occur in the spectroscopy important region 1.7−2.4 Å) there are also secondary maxima in the curves M_x (dashed lines in Figure 4). At very short O−Cl distance (1.6 Å) the M_x transition moment starts to grow (Figure 4) because the T_2 and S_1 potential energy curves are getting closer, but it does not contribute much to the absorption cross-section. In spite of the different behavior of the $M_x(T^y)$ component in different basis sets, the total oscillator strength of the vertical $T_2 \leftarrow S_0$ transition in the HOCl molecule does not depend much on the method used (Table 5).

The similar behavior is obtained for the M_x transition dipole moments in the HOBr molecule (dashed lines in Figure 7). The growth at r(O−Br) = 1.6 Å also occurs by the same process as that for the HOCl molecule, and two maxima are well seen for longer O−X distances (2.15 and 2.35 Å, respectively). The states T_2 ($1^3A'$) and S_1 ($1^1A''$) are well separated in this region in HOBr, so there is no suspect for applicability of perturbation theory. In the HOBr molecule the in-plane polarization of the $T_2 \leftarrow S_0$ absorption prevails over the out-of-plane polarization in the whole region of the studied O−Br distances. The total transition dipole moment vector has almost constant orientation (at least in the Franck−Condon region); it comes out of plane, but has the largest projection along the O−Br axis.

In HOI molecule the growth of the perpendicular polarization components of the T_2-S_0 transition moment (dashed lines in Figure 10) at very short O−I distance (2.1 Å) seems also to be artificial. The T_2 and S_1 energy levels are separated (Figure 8)

TABLE 9: Vertical Excitation Energies (ΔE/eV) and Oscillator Strengths (in Parentheses) for the Singlet−Singlet and Singlet−Triplet Transitions in the HOCl, HOBr, and HOI Molecules

HOCl

state	aug-cc-pVDZ	Sadlej	3-21 G	MRCI[a]	CI[b]	exptl[c]
$1^3A''$	2.95 (5.43 × 10⁻⁶)	2.91 (5.7 × 10⁻⁶)	3.23 (3.94 × 10⁻⁶)	3.47		3.26[d]
$1^3A'$	3.93(3.15 × 10⁻⁵)	3.92 (3.74 × 10⁻⁵)	4.59 (8.19 × 10⁻⁶)	4.68		~4.07[e]
$1^1A''$	4.08 (6.9 × 10⁻⁴)	4.03 (6.1 × 10⁻⁴)	4.56 (1.1 × 10⁻⁴)	4.51 (1.9 × 10⁻⁵)	4.02	4.07[e]
$2^1A'$	5.18 (2.07 × 10⁻³)	5.13 (1.7 × 10⁻³)	5.46 (1.55 × 10⁻³)	5.68 (1.7 × 10⁻³)	5.16	5.12
$2^1A''$	6.50 (0)	6.18 (0)	6.44 (0)		6.77	
$3^1A''$	7.24 (5.58 × 10⁻³)	7.17 (5.6 × 10⁻³)	7.52 (5.37 × 10⁻³)	7.75 (6.2 × 10⁻³)	8.6	
$3^1A'$	9.26 (0)	8.99 (0)	9.11 (0)		8.01	
$4^1A'$	9.45 (3.80 × 10⁻²)	9.36 (3.2 × 10⁻²)		9.69 (8.12 × 10⁻²)		

HOBr

state	AhlrichsVDZ	Sadlej	3-21 G	CIS[a]	MRCI[a]	exptl[f]
$1^3A''$	2.90 (8.4 × 10⁻⁵)	2.64 (7.28 × 10⁻⁵)	3.07 (4.86 × 10⁻⁵)	2.95	2.48	2.82[g]
$1^3A'$	3.73(7.38 × 10⁻⁴)	3.43 (2.01 × 10⁻⁴)	4.16 (3.78 × 10⁻⁴)	3.72	3.44	~3.5[e]
$1^1A''$	3.86 (6.59 × 10⁻⁴)	3.69 (3.76 × 10⁻⁴)	4.00 (1.07 × 10⁻³)	4.16 (6 × 10⁻⁴)	3.29 (1.8 × 10⁻⁶)	3.54[e]
$2^1A'$	4.89 (5.21 × 10⁻³)	4.60 (1.74 × 10⁻³)	5.22 (4.76 × 10⁻³)	5.08 (5.50 × 10⁻³)	4.24 (1.00 × 10⁻³)	4.43
$2^1A''$	6.13 (0)	6.78 (0)	5.65 (0)		6.77	
$3^1A''$	6.73 (7.15 × 10⁻³)	6.82 (5.16 × 10⁻³)	8.92 (0)	7.89 (8.90 × 10⁻³)	5.57 (3.70 × 10⁻³)	
$3^1A'$	8.41 (0)	8.57 (6.89 × 10⁻²)	8.05 (0)	8.01	8.34	
$4^1A'$	8.92 (2.99 × 10⁻¹)	8.94 (2.90 × 10⁻¹)	9.12 (2.44 × 10⁻¹)			

HOI

state	3-21G (exptl)[h]	3-21 (opt)[i]	exptl[j]
$1^3A''$	2.73 (2.46 × 10⁻⁴)	2.28 (1.6 × 10⁻⁴)	
$1^3A'$	3.58 (5 × 10⁻³)	3.12(3.09 × 10⁻³)	3.1[e]
$1^1A''$	3.57 (2.4 × 10⁻³)	3.03 (9.03 × 10⁻⁴)	3.1[e]
$2^1A'$	4.60 (6.71 × 10⁻³)	4.02 (3.64 × 10⁻³)	4.43
$2^1A''$	6.30 (1.18 × 10⁻²)	4.62 (0)	
$3^1A''$	6.79 (0)	5.18 (6.43 × 10⁻³)	
$3^1A'$	8.27 (4.42 × 10⁻¹)	6.20 (0)	
$4^1A'$	8.73 (0)	7.53 (2.90 × 10⁻¹)	

[a] Reference 3. [b] Reference 25. [c] Reference 20. [d] Reference 5. [e] Two overlapping bands. [f] Reference 29. [g] Reference 4. [h] Calculated at the experimental geometry. [i] Calculated at the optimized geometry. [j] Reference 2.

by 0.09 eV (726 cm⁻¹) at the ground state optmizaed geometry (Table 9); this energy gap is comparable with the SOC integral,[30] which is equal 1377 cm⁻¹ for $b = y$, so the perturbation theory is not applicable. Starting from the point $r(O-I) = 2.15$ Å, the integral eq 31 has been substituted by $1/\sqrt{2}\langle 1^1A'|e\sum_i x_i|1^1A''\rangle = 0.08$ au, by taking into account that both transitions $S_1 \leftarrow S_0$ and $T_2 \leftarrow S_0$ share the same intensity when they are totally mixed by SOC.

Besides this artificial large increase of the $M_x(T^y)$ integral at short O−I distances, the $M_y(T^x)$ transition moment (solid line in Figure 10) is pretty constant in the whole range of the dissociation reaction coordinate studied in this work; it is about 0.075 au. This result does not depend on shortcomings of the QR scheme and is quite reliable. Even this $M_y(T^x)$ transition moment provides a strong absorption intensity, so the out-of-plane polarized $S_1 \leftarrow S_0$ band ($M_x = 0.11$ au) in the HOI molecule should be overlapped with the mixed polarized $T_2 \leftarrow S_0$ band; the total cross-section should be increased twice as much, at least, independently on the possible artificial overestimation of the $M_x(T^y)$ integral at short O−I distances.

2. T_2-S_0 ($1^3A' \leftarrow 1^1A'$) Transitions to the x Spin Sublevel. According to eqs 21−24, these transitions are in-plane (y, z) polarized. All calculations show (Tables 6−8) that this absorption has predominantly y polarization and is oriented along the O−Cl, O−Br, and O−I axes. (Compare the solid lines in Figures 4, 7, and 10.) The transition moment $M_y(T^x)$ for the HOCl molecule (Figure 4) is on the order of 0.01 au in all basis sets, which is on the order of typical spin-allowed S−S transitions. The transition moment $M_y(T^x)$ for the HOCl molecule has its maximum near the Franck−Condon region (Figure 4), so it produces a great contribution to the $T_2 \leftarrow S_0$ absorption cross-

section. Similar behavior is obtained for the HOBr molecule (Figure 7) in Sadlej and 3-21G basis sets (Table 7). In HOI the $T_2 \leftarrow S_0$ transition moment $M_y(T^x)$ is the largest one starting with $r(O-I) \geq 2.2$ Å (Figure 10). The z polarization (O−H bond direction) is less intense in all molecules (Figures 4, 7, and 10, Tables 6−8).

As was mentioned before, the considered second $T_2 \leftarrow S_0$ transition enters the region of the first $S_1 \leftarrow S_0$ absorption in the HOCl molecule; in the HOBr molecule the T_2 state is lower in energy than the S_1 one by 0.26 eV (Table 9, Sadlej basis set). The intrusion problem of the quasi-degeneracy of the T_2 and S_1 states is not so dramatic in the HOBr molecule as that in the HOCl. At the same time the calculated oscillator strength for the $T_2 \leftarrow S_0$ vertical transition in the HOBr molecule is pretty high ($f = 2 \times 10^{-4}$, Sadlej basis set) with 70% of the intensity polarized along the O−Br axis. Although the in-plane/out-of-plane polarization ratio strongly depends on the basis set used (Tables 6 and 7), a strong in-plane component (O−Cl and O−Br axes) is definitely present in the $T_2 \leftarrow S_0$ absorption. This is in great contrast with the $S_1 \leftarrow S_0$ absorption which is entirely out-of-plane polarized. So the first intense near-UV absorption band, $\lambda_{max} = 304$ nm in HOCl[5,20] and $\lambda_{max} = 350$ nm in HOBr,[4,60] should consist of two transitions, $T_2 \leftarrow S_0$ and $S_1 \leftarrow S_0$, with different polarization.

For vertical excitations the $T_2 \leftarrow S_0$ transition has a larger intensity than the $S_1 \leftarrow S_0$ one in the HOBr and HOI molecules. The only exception is obtained for the Sadlej basis set, Table 7. The exception is not unexpected since the $S_1 \leftarrow S_0$ intensity strongly depends on the O−X distance. For example, the $S_1 \leftarrow S_0$ transition moment (M_x) increases with larger O−Cl separations (from 0.0007 au at the equilibrium point up to 0.03 au at

$r_{O-Cl} = 2$ Å, cc-pVDZ). This behavior determines a wide diffuse absorption band in the HOCL spectrum ($\lambda_{max} = 304$ nm) as a shoulder of more strong peak at $\lambda_{max} = 242$ nm (the $S_2 \leftarrow S_0$ transition).[20,25] A similar trend (Tables 6 and 7) corresponds to the UV absorption spectrum of the HOBr molecule.[60] The $S_1 \leftarrow S_0$ transition moment is a widespread function of O−Br distance with a maximum value 0.09 au at $r_{O-Br} = 2.3$ Å. A diffuse absorption band in the HOBr spectrum ($\lambda_{max} = 350$ nm) determined by this $S_1 \leftarrow S_0$ transition has a significant contribution from the $T_2 \leftarrow S_0$ excitation. Both transition moments are increasing functions of the O−Br distance in the Franck−Condon region. The function $M_y(T^x)$ is more steep (Figure 7) than the S−S transition moment function and has a maximum at shorter distance $r_{O-Br} = 2.06$ Å, which is closer to the Franck−Condon region. The $S_1 \leftarrow S_0$ transition moment ($M_x = 0.06$ au) is comparable with the total $T_2 \leftarrow S_0$ transition moment ($|M| = 0.049$ au) for the vertical excitations. Both transitions are almost equally important for the intensity of the absorption band at 350 nm in the HOBr molecule and produce a wide non-Gaussian contour with nonhomogeneous features. Comparison of the 304 and 350 nm bands in the HOCl and HOBr molecules, respectively,[2] clearly indicate that the $S_1 \leftarrow S_0$ transition in hypobromous acid is much more perturbed by the overlapping $T_2 \leftarrow S_0$ transition than that in hypochlorous acid. This is in good qualitative agreement with the results of Table 9 for both molecules (compare the 3-21G and Sadlej basis set results for HOCl and HOBr).

The absorption spectrum of HOI molecule presented in ref 2 consists from two maxima: the first absorption band at 410 nm is more intense than the short wavelength band with maximum at 338 nm. (The $T_1 \leftarrow S_0$ absorption seems to be overlapped by a wide intense band with maximum at 410 nm.) Both the $T_2 \leftarrow S_0$ and $S_1 \leftarrow S_0$ transitions come to the region of 410 nm absorption band (Table 9). Comparison of the 3-21G basis set calculations for all three molecules (Table 9) shows that the $T_2 \leftarrow S_0$ transition is getting more intense in the row Cl < Br < I. A strong red shift of the $T_2 \leftarrow S_0$ band going from X = Cl, Br to X = I is also reproduced (Table 9). The intensity increase of the 410 nm band in the HOI molecule is in qualitative agreement with the general trend of the UV−vis absorption spectra genesis of all three molecules.[2]

The calculated $T_2 \leftarrow S_0$ ($1^3A' \leftarrow 1^1A'$) transition moment has strong components along both y and x axes, so the result cannot be considered as an artifact of perturbation theory. For example, calculation of the vertical transition intensity in the HOCl molecule in the cc-pVDZ basis set gives a rather small perpendicular component $M_x^2 = 9 \times 10^{-6}$ but a very large transition moment along the O−Cl axis $M_y^2 = 8.8 \times 10^{-5}$. It means that the intensity is borrowed mostly from the $n^1A' \leftarrow 1^1A'$ transitions (in part from the $S_2 \leftarrow S_0$ band at 242 nm). The oscillator strengths for the $T_2 \leftarrow S_0$ ($1^3A' \leftarrow 1^1A'$) transition in the HOCl molecule calculated in the cc-pVDZ and Ahlrichs-VDZ basis sets (1.04×10^{-5} and 2.15×10^{-5}, respectively) are very close to the f values presented in Table 9. The result is very stable with respect to the basis set and active space expansion though the $1^1A'' \leftarrow 1^1A'$ transition intensity indeed is quite sensitive to the basis set (Table 9, HOCl molecule) and to small displacements along the O−Cl bond length. This also indicates the applicability of the quadratic response method for the $1^3A' \leftarrow 1^1A'$ transition intensity calculation. The new calculations confirm the previous result[28] for the $T_2 \leftarrow S_0$ absorption in both molecules.

Comparing the $T_2 \leftarrow S_0$ transition moments in all three molecules, one can say that in HOCl the out-of-plane polariza-

tion prevails over the in-plane polarization if we shall take into account the results of the largest (Sadlej, aug-cc-pVDZ) basis sets (Table 6), and this is vice versa in the HOBr molecule. In HOBr the total transition dipole moment vector has almost constant orientation (at least in the Franck−Condon region); it comes out of plane, but has the largest projection along the O−Br axis. In the HOI molecule the out-of-plane polarization prevails over the in-plane polarization just for the vertical excitation; the total transition dipole moment vector rapidly comes to the molecular plane during first steps of the dissociation process. The in-plane component is almost parallel to the O−I axis and is a slow declining function of the O−I distance.

3. Angle Dependence of the $T_2 \leftarrow S_0$ ($1^3A' \leftarrow 1^1A'$) Transition Moment and the Absorption Cross-Section. The perpendicular component rapidly diminishes with increasing bending angle in both molecules. For example, in the HOCl species the $M_x(T^y)$ integral falls from the value 0.0028 au at the equilibrium ($\angle HOCl = 100.8°$) to $M_x(T^y) = 0.0015$ au at the angle $\angle HOCl = 110°$ and then to $M_x(T^y) = 0.0002$ au at the angle $\angle HOCl = 120°$ (the cc-pVDZ results). A similar behavior characterizes the $M_x(T^z)$ component. So the intensity borrowing from the $1^1A'' \leftarrow 1^1A'$ transition becomes completely unimportant when the angle increases. At the same time the in-plane polarized transition intensity does not change much. There is only a redistribution between $M_y(T^x)$ and $M_z(T^x)$ components. The transition moment $M_a(T^x)$ is almost parallel to the O−Cl bond and O−Br bond directions. Since the behavior of the main contribution [the $1^3A'(T^x) \leftarrow 1^1A'$ transition moment] in relation to the intensity does not depend on the bending angle, we have neglected the angle dependence in the $T_2 \leftarrow S_0$ cross-section. The O−H stretching vibration seems to be not important for the $T_2 \leftarrow S_0$ transition intensity. Only the dependence on the O−X distance is here taken into account. This approach is questionable for the $T_2 \leftarrow S_0$ transition, especially in the HOCl molecule, so results have only semiquantitative meaning. The calculated $\sigma(\nu)$ function with the transition moment from Sadlej's basis set has a maximum $\sigma = 2.1 \times 10^{-20}$ cm² at $\nu \simeq 32\,500$ cm⁻¹ for the HOCl molecule and $\sigma = 7.9 \times 10^{-20}$ cm² at $\nu \simeq 28\,000$ cm⁻¹ for the HOBr species. Not only vertical transitions contribute to the absorption cross-section since the upper triplet state is dissociative. An account of the geometry dependence of transition dipole moments and the appropriate treatment for the nuclear wave functions leads to broad peaks, which being combined with the S−S absorption[25,26] produce better agreement with experiments for the HOCl spectrum in the region 290−320 nm.[7,18,20] For the HOI molecule, $\sigma = 1.8 \times 10^{-19}$ cm² at $\nu \simeq 25\,000$ cm⁻¹.

E. Comparison of the $T_1 \leftarrow S_0$ Absorption in Hypohalous Acids and in Water Molecules. It is relevant to compare the UV photodissociation of the H_2O molecule (the lightest member of the series X = H) with the hypohalous acids (HOX, X = Cl, Br, I) behavior. Recent[61] similar MCSCF QR calculations (aug-cc-pVDZ basis) determined that the first $T_1 \leftarrow S_0$ ($a^3B_1 \leftarrow X^1A_1$) absorption in water molecules also contributes to the photodissociation of H_2O at the UV long-wavelength tail (180−190 nm). The $a^3B_1 \leftarrow X^1A_1$ transition dipole moment has its maximum value ($M_{in-plane} = 0.003$ au) just near the vertical excitation. It slightly increases along the dissociation coordinate (this is analogous of the $1^3A'' \leftarrow 1^1A'$ transition studied above) until the distance $r_{O-H} = 1.6$ Å and then decreases rapidly to 0.0005 au at $r_{O-H} = 3$ Å. The out-of-plane polarization ($M_x(T^x)$ is negligible as in all hypohalous acids. Such $T_1 \leftarrow S_0$ absorption might explain the surprisingly small OD/OH ratio in the photodissociation of DOH at 193 nm.[62] This wavelength is at

the long wavelength side of the water absorption spectrum ($\lambda_{max} \sim 165$ nm); the cross-section is extremely small here. So any small changes in the wave functions can give a dramatic effect on the photodissociation of the H_2O molecule in this region. Excitation at 193 nm accesses the upper singlet state PEC far away from the Franck–Condon region of nuclear coordinates. Therefore the absorption cross-section at 193 nm is determined by the tiny overlap of the continuum wave functions in the upper state with the exponentially decaying tails of the initial ground state nuclear wave function. Because of the lighter mass of the H atom, the OH stretches significantly further out into the H–OD channel than the OD bond does into the HO–D exit channel. For these reasons, the H–OD channel is easily excited by low-energy photons in comparison with the HO–D channel, so the H + OD/D + OH branching ratio in the photodissociation of DOH at low-energy photons (193 nm) should be very large as predicted by calculations which take into account only the singlet–singlet absorption.[62] The measured ratio is an order of magnitude smaller than the theory predicts.[63] Along the same lines the theory predicts that the absorption cross-section at 193 nm for H_2O should be about 200 times larger than for D_2O,[62] but experiment gives a value of only 64 ± 8.[63] All of these striking discrepancies can be explained if the $T_1 \leftarrow S_0$ ($^3B_1 \leftarrow X^1A_1$) absorption in water molecules is taken into account. In order to explain the observed OD/OH ratio, the $^3B_1 \leftarrow X^1A_1$ transition dipole moment of about 0.015 au was inferred,[62] which is in semiquantitative agreement with our prediction (0.003 au). Account of the $\angle HOH$ angle variation increases the transition dipole moment value (this work is under the progress). The above-mentioned features could be applied for isotope effects in hypohalous acids photodissociation. The calculated absorption cross-section of the $T_1 \leftarrow S_0$ transition in water at 193 nm ($\sigma = 3.2 \times 10^{-21}$ cm^2) is very similar to that of the hypochlorous acid at the first absorption band near 380 nm.

IV. Conclusions

The following conclusions about the long wavelength absorption of hypochlorous, hypobromous, and hypoiodous acids have been obtained in this MCSCF QR study, which could be important for the understanding the role of these molecules in stratospheric photochemistry.

The first $T_1 \leftarrow S_0$ ($1^3A'' \leftarrow 1^1A'$) transition in the HOCl molecule produces a weak diffuse peak (long-wave shoulder) at $\lambda_{max} \sim (385-420)$ nm (depending on basis set used) with an oscillator strength $f \sim (5-6) \times 10^{-6}$, which is about 2 orders of magnitude less intense in comparison with the first singlet–singlet absorption at $\lambda_{max} \sim 304$ nm. (The last band intensity strongly depends on basis set and geometry.) The $T_1 \leftarrow S_0$ absorption band borrows intensity from the UV transitions of the $n^1A' \leftarrow 1^1A'$ type and has a strong polarization along the O–Cl bond (y axis) direction. It is connected mostly with the z spin sublevel (zero spin projection on the O–H direction) of the triplet state. These results are in perfect agreement with recent measurements of OH photofragment yields and of their Doppler line shapes.[5] Not only intensity of the $T_1 \leftarrow S_0$ absorption (the measured cross-section $\sigma = 4 \times 10^{-21}$ cm^2 [5]) but also polarization of the absorbing light obtained from the sub-Doppler spectroscopy (the O–Cl bond direction)[5] coincide with our previous prediction,[28] which is supported by the present study.

The second $T_2 \leftarrow S_0$ transition overlaps the energy region of the first $S_1 \leftarrow S_0$ absorption (the observed $\lambda_{max} \sim 304$ nm). Considering vertical excitations intensity one can say that the $T_2 \leftarrow S_0$ transition in the HOCl molecule is an order of

magnitude less intense than the $S_1 \leftarrow S_0$ one. The $S_1 \leftarrow S_0$ transition moment (M_x) increases with larger O–Cl separations, and this behavior determines a wide diffuse absorption band ($\lambda_{max} = 304$ nm) as a shoulder of a very strong peak at $\lambda_{max} = 242$ nm ($S_2 \leftarrow S_0$ transition).[20,25] Although the energies of the $1^3A'$ and $1^1A''$ states are very close in the Franck–Condon region, there is no large intensity borrowing from the $S_1 \leftarrow S_0$ transition with perpendicular polarization in the HOBr molecule. The calculated $T_2 \leftarrow S_0$ transition moment has stronger component along the y axis (O–Br bond direction), so it borrows intensity mainly from the strong second S–S absorption band at $\lambda_{max} = 280$ nm and from other $n^1A' \leftarrow 1^1A'$ transitions in the far-UV region. The similar arguments are applied for the HOCl molecule, but in this case the out-of-plane polarization slightly prevails over the in-plane (O–Cl axis) polarized light. So the intensity borrowing from the $S_1 \leftarrow S_0$ transition is more efficient for hypochlorous acid. Such intensity redistribution between the S–S and T–S transitions seems to be a real physical effect which should be taken into account for the interpretation of the long-wave absorption of the HOCl molecule since it leads to higher absorbance of the long-wave band (304 nm) and to significant changes in polarization and in distribution of the spin–orbit products OH($^2\Pi_{3/2,1/2}$) + Cl(^2P_J).

These effects are much stronger in the HOBr molecule. The formally calculated oscillator strength for the first $T_1 \leftarrow S_0$ transition ($1^3A'' \leftarrow 1^1A'$) is about 8×10^{-5}, so it is easily observed in the absorption spectrum at 440 nm.[3,4] The next $T_2 \leftarrow S_0$ transition is more intense and enters also in the region of the first $S_1 \leftarrow S_0$ absorption ($\lambda_{max} \sim 350$ nm) of hypobromous acid.[3,4] The MCSCF QR calculations predict $f = (2-7) \times 10^{-4}$ which is comparable or even larger than the oscillator strength of the $S_1 \leftarrow S_0$ transition itself. These findings qualitatively agree with intensity measurements of the long-wave absorption in the HOCl[5] and HOBr molecules.[4] The long-wave band (350 nm) of hypobromous acid is more intense and more wide than the 304 nm band of hypochlorous acid;[2] it also demonstrates some nonhomogeneous feature which indicate that this absorption is a mixture of two transitions.

The calculated singlet–triplet absorption in hypoiodous acid is more intense than in hypobromous acid. Comparison made in the same basis set (3-21G) shows that the $T_1 \leftarrow S_0$ transition is twice as much more intense in HOI than in HOBr. But this transition in HOI is overlapped by a very intensive absorption band at 410 nm, which probably consists from the $S_1 \leftarrow S_0$ and $T_2 \leftarrow S_0$ transitions. The HOI spectrum presented in ref 2 consists from two maxima; in contrast to the spectra of hypochlorous and hypobromous acids, the absorption spectrum of HOI molecule has an intense first peak in the visible region at 410 nm and the weaker second peak at 335 nm.[2] Calculated spectra (Table 9) qualitatively agree with such findings, although the great increase of the $T_2 \leftarrow S_0$ transition intensity seems to be overestimated by perturbation theory. A strong red shift of the $T_2 \leftarrow S_0$ band going from X = Cl, Br to X = I is well reproduced in 3-21G basis.

Absorption by the first and second excited triplet states of hypochlorous, hypobromous, and hypoiodous acids makes an important contribution to the overall atmospheric photochemical activity of these molecules. Accounting for the importance of the T–S transitions in spectra and reactivity of ozone itself[33,36,39] for the possible involvement of the triplet states in processes 1–4 and in the similar reactions with the bromine and iodine counterparts, we make the general conclusion that photochemistry of the triplet states should be an important issue in the stratospheric ozone problem. The present results suggest that

atmospheric photochemistry of the heavy halogen (bromine and, particularly, iodine) containing compounds would strongly depend on the singlet−triplet transitions and on account of relativistic effects. Thermochemical ab initio calculations of BrO− and IO− anions[64,65] (possible products of the hypobromous and hypoiodous acids dissociation and their isoelectronic analogous) indicate that these species are pretty stable in their ground singlet state. Our calculations with SOC account show that these species are entirely unstable because the singlet $^1\Sigma^+$ state potential energy curve is crossed just near the minimum by the triplet $^3\Pi$ state curve which is repulsive. Spin−orbit coupling matrix element between these S and T states in the crossing point is quite large so the molecules are predissociative in the gas phase.

The SOC effects and the S−T transitions are important even in photochemistry of such light molecules like water. The $T_1 \leftarrow S_0$ absorption might explain the surprisingly small OD/OH ratio in the photodissociation of HOD at 193 nm.[62] This excitation corresponds to a nonvertical transition. Therefore the absorption cross-section at 193 nm is determined by the tiny overlap of the continuum wave functions in the upper state with the weak tail of the ground state vibrations. In order to explain the observed OD/OH ratio the $^3B_1 \leftarrow X^1A_1$ transition dipole moment of about 0.04 Debye was inferred,[62] which is in semiquantitative agreement with our prediction (0.008 Debye) obtained by the same approximation used for hypohalous acids. Similar prediction could be obtained for isotope effects in O_3, HOCl, and HOBr photodissociation.

Because hypochlorous and hypobromous acids play an important role in the partitioning of chlorine and bromine in the stratosphere, the $T_1 \leftarrow S_0$ absorption may contribute significantly to the distribution of chlorine and bromine species at altitudes above the tropopause.[5] Estimations show[4,5] that absorption in the triplet band previously neglected reduces the instantaneous lifetime of hypochlorous and hypobromous acids and their stratospheric abundance. An intense visible absorption and photodissociation of hypoiodous acid by the S−T transitions cannot show that this species is an effective reservoir in the troposphere.

References and Notes

(1) Rowland, F. S.; Molina, M. J. *Rev. Geophys.* **1975**, *13*, 21.
(2) Wayne, R. P. *Atmos. Environ.* **1995**, *29*, 2675.
(3) Francisco, J. S.; Hand, M. R.; Williams, I. H. *J. Phys. Chem.* **1996**, *100*, 9250.
(4) Barnes, R. J.; Lock, M.; Coleman, J.; Sinha, A. *J. Phys. Chem.* **1996**, *100*, 453.
(5) Barnes, R. J.; Sinha, A.; Michelsen, H. A. *J. Phys. Chem. A* **1998**, *102*, 8855.
(6) Molina, L. T.; Molina, M. J. *J. Phys. Chem.* **1978**, *82*, 2410.
(7) Molina, L. T.; Ishiwata, T.; Molina, M. J. *J. Phys. Chem.* **1980**, *84*, 821.
(8) Fan, S. M.; Jacob, D. J. *Nature* **1992**, *359*, 522.
(9) Hanson, D. R.; Ravishankara, A. R. *Geophys. Res. Lett.* **1995**, *22*, 385.
(10) Klaassen, J. J.; Lindner, J.; Leone, S. R. *J. Chem. Phys.* **1996**, *104*, 7403.
(11) Solomon, S.; Garcia, R. R.; Ravishankara, A. R. *J. Geophys. Res.* **1994**, *99*, 20491.
(12) Solomon, S.; Burkholder, J. B.; Garcia, R. R.; Ravishankara, A. R. *J. Geophys. Res.* **1994**, *99*, 20929.
(13) Barnes, R. J.; Becker, K. H.; Starke, J. *Chem. Phys. Lett.* **1992**, *196*, 578.
(14) Jenkin, M. E.; Cox, R. A.; Hayman, G. D. *Chem. Phys. Lett.* **1991**, *177*, 272.
(15) Mishalanie, E. A.; Rutkowski, C. J.; Hutte, R. S.; Birks, J. W. *J. Phys. Chem.* **1986**, *90*, 5578.

(16) Jaffe, S.; DeMore, W. B. *NASA Ref. Publ.* **1977**, *1010*, 1.
(17) Butler, P. J. D.; Fhillips, L. F. *J. Phys. Chem.* **1983**, *80*, 183.
(18) Knauth, H. D.; Alberti, H.; Clausen, H. *J. Phys. Chem.* **1979**, *87*, 183.
(19) Permien, T.; Vogt, R.; Schindler, R. N. *Air Pollut. Rep.* **1988**, *17*, 149.
(20) Burkholder, J. B. *J. Geophys. Res.* **1993**, *98*, 2963.
(21) Jaffe, R. L.; Langhoff, S. R. *J. Chem. Phys.* **1978**, *68*, 1639.
(22) Hirsch, G.; Bruna, P. J.; Peyerimhoff, S. D.; Buenker, R. J. *Chem. Phys. Lett.* **1977**, *52*, 442.
(23) Bruna, P. J.; Hirsch, G.; Peyerimhoff, S. D.; Buenker, R. J. *Can. J. Chem.* **1979**, *57*, 1839.
(24) Nanbu, S.; Nakata, K.; Iwata, S. *Chem. Phys.* **1989**, *135*, 75.
(25) Nanbu, S.; Iwata, S. *J. Phys. Chem.* **1992**, *96*, 2103.
(26) Guo, H. *J. Phys. Chem.* **1993**, *97*, 2602.
(27) Offer, A. R.; Balint-Kurti, G. G. *J. Chem. Phys.* **1994**, *101*, 10416.
(28) Minaev, B. F.; Ågren, H. *J. Chem. Soc., Faraday Trans.* **1998**, *94*, 2061.
(29) Orlando, J. J.; Burkholder, J. B. *J. Phys. Chem.* **1995**, *99*, 1143.
(30) Palmer, D. A.; van Eldik, R. *Inorg. Chem.* **1986**, *25*, 928.
(31) Stevens, J. E.; Cui, Q.; Morokuma, K. *J. Chem. Phys.* **1998**, *108*, 1544.
(32) Bouvier, A. J.; Bacis, R.; Bussery, B. *Chem. Phys. Lett.* **1996**, *255*, 263.
(33) Minaev, B. F.; Ågren, H. *Chem. Phys. Lett.* **1994**, *217*, 531.
(34) Koput, J.; Peterson, K. A. *Chem. Phys. Lett.* **1998**, *283*, 139.
(35) Skokov, S.; Peterson, K. A.; Bowman, J. M. *J. Chem. Phys.* **1998**, *109*, 2662.
(36) Bacis, R.; Bouvier, A. J.; Flaud, J. M. *Spectrochim. Acta, Part A* **1998**, *54*, 17.
(37) Gunther, J.; Anderson, S. M.; Hilpert, G.; Mauersberger, K. *J. Chem. Phys.* **1998**, *108*, 5449.
(38) Braunstein, M.; Martin, R. L.; Hay, P. J. *J. Chem. Phys.* **1995**, *102*, 3662.
(39) Minaev, B. F.; Kozlo, E. M. *Theor. Exp. Chem.* **1997**, *33*, 219.
(40) Jørgensen, P.; Olsen, J.; Jensen, H. J. Aa. *J. Chem. Phys.* **1988**, *74*, 265.
(41) Hettema, H.; Jensen, H. J. Aa.; Jørgensen, P.; Olsen, J. *J. Chem. Phys.* **1992**, *97*, 1174.
(42) Vahtras, O.; Ågren, H.; Jørgensen, P.; Jensen, H. J. Aa.; Helgaker, T.; Olsen, J. *J. Chem. Phys.* **1992**, *97*, 9178.
(43) Ågren, H.; Vahtras, O.; Minaev, B. F. *Adv. Quantum Chem.* **1996**, *27*, 71.
(44) Langhoff, S. R.; Davidson, E. R. *J. Chem. Phys.* **1976**, *64*, 4699.
(45) Klotz, R.; Marian, C. M.; Peyerimhoff, S. D.; Hess, B. A.; Buenker, R. J. *Chem. Phys.* **1984**, *89*, 223.
(46) Yarkony, D. R. *Int. Rev. Phys. Chem.* **1992**, *11*, 195.
(47) Minaev, B. F. *Fizika Molekul, Naukova Dumka, Kiev* **1979**, *7*, 34.
(48) Olsen, J.; Jørgensen, P. *J. Chem. Phys.* **1985**, *82*, 3235.
(49) Woon, D. E.; Dunning, T. H. *J. Chem. Phys.* **1993**, *98*, 1358.
(50) Sadlej, A. J. *Theor. Chim. Acta* **1991**, *79*, 123.
(51) Schafer, A.; Horn, H.; Ahlrichs, R. *J. Chem. Phys.* **1992**, *97*, 2571.
(52) Binkley, J. S.; Hehre, W. J.; Pople, J. A. *J. Am. Chem. Soc.* **1980**, *102*, 939.
(53) Lee, T. J. *J. Phys. Chem.* **1994**, *98*, 3697.
(54) Deeley, C. M. *J. Mol. Struct. (THEOCHEM)* **1987**, *122*, 481.
(55) Dewar, M. J. S.; Thiel, W. *J. Am. Chem. Soc.* **1977**, *99*, 4899.
(56) Turner, A. G. *Chem. Phys. Lett.* **1986**, *125*, 451.
(57) Goddard, W. A., III; Dunning, T. H., Jr.; Hunt, W. J.; Hay, P. J. *Acc. Chem. Res.* **1973**, *6*, 368.
(58) Bell, A. J.; Boggis, S. A.; Dyke, J. M.; Frey, J. G.; Richter, R.; Shaw, N. S. *J. Chem. Soc., Faraday Trans.* **1994**, *90*, 17.
(59) Hickman, C. G.; Shaw, N. S.; Crawford, M. J.; Bell, A. J.; Frey, J. G. *J. Chem. Soc., Faraday Trans.* **1993**, *89*, 1623.
(60) Orlando, J. J.; Burkholder, J. B. *J. Phys. Chem.* **1995**, *99*, 1143.
(61) Minaev, B. F.; Ågren, H. *J. Mol. Struct. (THEOCHEM)* **1998**, *0*, 00.
(62) Schröder, T.; Schinke, R.; Ehara, M.; Yamashita, K. *J. Chem. Phys.* **1998**, *109*, 6641.
(63) Plusquellic, D. F.; Votava, O.; Nesbitt, D. J. *J. Chem. Phys.* **1998**, *109*, 6633.
(64) Glukhovtsev, M. N.; Pross, A.; Radom, L. *J. Phys. Chem.* **1996**, *100*, 3498.
(65) Hassanzadeh, P.; Irikura, K. K. *J. Phys. Chem. A* **1997**, *101*, 1580.
(66) Lee, T. J. *J. Phys. Chem.* **1995**, *99*, 15074.
(67) Recently reactions of the OH and O(^{3}P) radicals with alkyl iodides are found to be effective methods of synthesizing HOI for spectral studies.[10,13] The role of spin−orbit coupling in these reactions is now well understood.[31]